Environmental Science
Processes & Impacts

# Integrated Experimental and Theoretical Approach to Probe the Synergistic Effect of Ammonia in Methanesulfonic Acid Reactions with Small Alkylamines



| | |
|---|---|
| Journal: | *Environmental Science: Processes & Impacts* |
| Manuscript ID | EM-ART-09-2019-000431.R2 |
| Article Type: | Paper |
| | |

# Integrated Experimental and Theoretical Approach to Probe the Synergistic Effect of Ammonia in Methanesulfonic Acid Reactions with Small Alkylamines

**Véronique Perraud,[1] Jing Xu,[2] R. Benny Gerber[1,3*] and B. J. Finlayson-Pitts[1**]**

[1]Department of Chemistry, University of California, Irvine, CA 92697, USA.

[2]Department of Optical Engineering, Zhejiang A&F University, Lin'an 311300 Zhejiang, China.

[3]Institute of Chemistry, The Fritz Haber Research Center, The Hebrew University of Jerusalem, Jerusalem 91904, Israel.

Revision for:

*Environmental Science: Processes & Impacts*

*Author to whom correspondence should be addressed for theory.
Email: bgerber@uci.edu; phone (949) 824-6758; FAX (949) 824-2420

**Author to whom correspondence should be addressed for experiments.
Email: bjfinlay@uci.edu; phone: (949) 824-7670; FAX (949) 824-2420

NH3 paper_Text_Final_Dec19.doc

# Abstract

While new particle formation events have been observed worldwide, our fundamental understanding of the precursors remains uncertain. It has been previously shown that small alkylamines and ammonia ($NH_3$) are key actors in sub-3 nm particle formation through reactions with acids such as sulfuric acid ($H_2SO_4$) and methanesulfonic acid ($CH_3S(O)(O)OH$, MSA), and that water also plays a role. Because $NH_3$ and amines co-exist in air, we carried out combined experimental and theoretical studies examining the influence of the addition of $NH_3$ on particle formation from the reactions of MSA with methylamine (MA) and trimethylamine (TMA). Experiments were performed in a 1-m flow reactor at 1 atm and 296 K. Measurements using a condensation particle counter (CPC) and a scanning mobility particle sizer (SMPS) show that new particle formation is systematically enhanced upon simultaneous addition of $NH_3$ to the MSA+amine binary system, with the magnitude depending on the amine investigated. For the MSA+TMA reaction system, the addition of $NH_3$ at ppb concentrations produces a much greater effect (i.e. order of magnitude more particles) than the addition of ~12,000 ppm water (corresponding to ~45-50% relative humidity). The effect of $NH_3$ on the MSA+MA system, which is already very efficient in forming particles on its own, is present but modest. Calculations of energies, partial charges and structures of small cluster models of the multi-component particles likewise suggest synergistic effects due to $NH_3$ in the presence of MSA and amine. The local minimum structures and the interactions involved suggest mechanisms for the synergistic effect.

# Environmental Significance

Acid-base chemistry between gas phase precursors is recognized as an important source of new particles in air. Previous experimental and theoretical calculations have shown that small alkylamines play a critical role in sub-3 nm particles through reactions with strong acids such as sulfuric acid and methanesulfonic acid (MSA), the latter originating from oxidation of organosulfur compounds. As the energy landscape is transitioning away from fossil fuel sulfur dioxide, MSA contribution to this chemistry is expected to be more important in the future. Alkylamines are ubiquitous in the atmosphere and they often co-exist with ammonia; thus synergism or competition between precursors may arise. This study highlights synergistic interactions between $NH_3$ and methylamine and trimethylamine in their reactions with MSA. Quantum calculations provide critical molecular insights into the central role that $NH_3$ plays in particle formation in these systems.

# Introduction

New particle formation (NPF), the process by which gas phase precursors combine to give birth to particles in air, has been observed all around the world.[1-4] Such events have been measured in polluted urban areas,[5-7] above forest canopies,[8-11] in marine environments[12-14] and Arctic regions.[15, 16] This phenomenon typically leads to the formation of stable molecular clusters that can further grow by uptake of trace gases and water to sizes sufficient to impact visibility,[17-19] public health[20-24] and climate.[25-28] Despite these observations, our understanding of the mechanisms of nucleation and growth is still limited, with many open experimental and theoretical challenges.

There are many types of particles in air, and their properties vary greatly depending on the molecular constituents. An important type of airborne particle is that resulting from acid:base chemistry, with sulfuric acid reactions with ammonia and amines recognized as being particularly important in NPF.[29-54] Other species such as water[42, 44, 55-58] and organics[6, 8, 11, 59-65] may also play a role in this chemistry. Acid:base systems involving $HNO_3$,[66-69], HCl[68, 70, 71] or small carboxylic acids[72-79] may contribute, although the interactions of the respective acids with ammonia and amines were found to be weaker than that with $H_2SO_4$.

Methanesulfonic acid ($CH_3S(O)(O)OH$, MSA), a strong acid (pKa = -1.9),[80] is often formed alongside $H_2SO_4$ from the photooxidation of organosulfur compounds in air.[81] Previous experimental and computational studies from our laboratory have demonstrated that reaction of MSA with small alkylamines can be a significant source of NPF in air.[73, 74, 82-85] If emissions of sulfur dioxide (precursor to $H_2SO_4$ in air) associated with fossil fuel combustion continues to decline in the future as expected,[86-91] the relative contribution from MSA compared to $H_2SO_4$ to NPF will increase.[88] The concentration of gas phase MSA can be 10-100% of that of current

$H_2SO_4$ concentrations,[92-99] and a role for MSA in particle formation is supported by field observations of MSA in smaller particles.[8, 11, 100-102]

Until now, most experimental and theoretical studies of acid:base particles have addressed particles made of one acid component (e.g. $H_2SO_4$ or MSA), and one base component ($NH_3$ or an amine), under dry or humid conditions. Enhancement of NPF due to small alkylamines was reported to be greater than that from $NH_3$ for both $H_2SO_4$[29-33, 37, 41, 48, 52, 54] and MSA reactions.[84] Additionally, amines have been observed to displace ammonia from clusters and particles for both acids.[67, 103-106] A few studies investigated multi-component acid:base combinations with more than one acid.[73, 74, 107-110] However, studies investigating multi-component acid:base clusters and particles in which *both* an amine and $NH_3$ are present simultaneously at the onset of the nucleation have been reported thus far only for $H_2SO_4$.[31, 32, 52, 111-114]

The present study adds to these recent findings with both experiments and quantum calculations for two specific MSA+amine+$NH_3$ systems, where the amines are a primary amine, methylamine (MA) and a tertiary amine, trimethylamine (TMA). These amines are both found in air along with $NH_3$.[115-118] The interactions in such systems are of fundamental and atmospheric interest. First, from a theoretical molecular point of view, one might expect proton transfer from the acid to the base to form a stable ion pair.[74, 119-121] Previous studies combining proton transfer calculations and experiments on the same systems[74, 119] suggest that proton transfer could be a good indicator for particle formation potential. For example, the MSA+MA system shows both proton transfer and high particle number concentrations, whereas, the MSA+$NH_3$ system exhibits no proton transfer under dry conditions, and is associated with little particle formation capacity. However, there are other factors to take into account as well, such

as the possibility of forming hydrogen bond networks between the species. Indeed, while the MSA+TMA system exhibits a proton transfer between the acid and the base, this system is not experimentally efficient at forming particles due to the lack of a hydrogen bond network connecting the ion pairs. For reported multi-component $H_2SO_4$-based particles that include both an amine and $NH_3$, the issue of competition between the two potential acceptors of the proton then arises.[112-114] Related to this is the question of whether a *synergy* between $NH_3$ and the amine affects particle growth.[112, 113] Under humid conditions, the issues are even more complex: does the presence of water molecules affect the efficiency of proton transfer or the synergism? How does it influence particle growth? These questions in such a complex system call for an integrated experimental and theoretical approach. This paper addresses these questions through experiments and calculations on multi-component MSA-based clusters, leading to insights into the location of the proton transfer and potential synergism between species with regards to particle formation.

This topic is also of significant relevance to NPF in the atmosphere. Gas phase amines and $NH_3$ are ubiquitous in air.[115] For example, they have been measured above oceans,[122, 123] at urban[124-128] and agricultural sites,[116-118, 129-132] from biomass burning,[117, 133] and from vegetation and forested areas.[126, 132, 134-136] Ammonia almost always co-exists with amines and its gas phase concentration is typically an order of magnitude higher than that of the amines. Both ammonium and aminium ions have been frequently measured in the same particles that contain significant amounts of methanesulfonate.[8, 11, 16, 100, 137-141] This study is also of particular significance as $NH_3$ is ubiquitous in air both outdoors and indoors[132, 142] due to its many sources, including human breath[143, 144] and water or gas supplies used in laboratory studies.[7, 29, 33, 34, 45, 53, 111, 145, 146]

# Experimental Methods

***1. Flow reactor description***. Formation of detectable (> 2.0 nm) nanoparticles was investigated using two 1-m borosilicate flow reactors over reaction times from 0.3 to 6 s at 296 K and 1 atm (Fig. 1). The characteristics of the flow reactors have been described elsewhere[73, 74, 83-85, 147] and details for both configurations are presented in the Supplementary Information (SI). Briefly, both reactors had fixed ring inlets at the upstream end of the reactor and spoked inlets mounted at the end of a set of movable concentric tubes. One reactor had three fixed ring inlets (rings A-C) located at the upstream end of the flow reactor and three spoked inlets (spokes 1-3) while the second had two fixed rings (rings A-B) and two movable spoked inlets (spokes 1-2). A total of ~17 L $min^{-1}$ of dry clean air flowed through the reactor and was distributed as follows: 13 L $min^{-1}$ was introduced at ring A, 1 L $min^{-1}$ (mixed with $NH_3$) was either introduced at ring B or spoke 1, with 2 L $min^{-1}$ at spoke 2 (MSA injection port) and 1 L $min^{-1}$ at spoke 3 (MA or TMA injection port). The flow reactor temperature was maintained at 296 K using a water jacket. Prior to each set of experiments, the flow reactor was cleaned with nanopure water and dried with dry clean air with the water jacket set at 343 K. The flow reactor was conditioned with a flow of gas phase MSA for at least two days prior to experiments.

These studies were performed using dry clean air provided by a purge air generator (Parker-Balston, model 75-62) followed by a purification system composed of carbon/alumina media (Perma Pure, LLC) and a 0.1 μm filter (DIF-N70; Headline Filters). To minimize contaminant $NH_3$ that might be present in purge air, in most experiments the entire 13 L $min^{-1}$ of the air feeding the first ring inlet (ring A) was passed through a trap containing phosphoric acid ($H_3PO_4$; ACS grade, EMD) coated glass beads followed by a drierite drying trap (anhydrous calcium sulfate, 100%; W. A. Hammmond Drierite Company LTD) prior to being added to the

flow tube. Note that it was not experimentally possible for the entire flow of purge air to be treated, but the 13 L $min^{-1}$ represents 76% of the total air flow. Blank measurements of air flowing through the reactor were performed by collecting air in custom-made cartridges containing 150 mg of glass wool as the sorbent material. The cartridges were extracted successively three times with 10 mL of 0.05 M oxalic acid aqueous solution followed by ion chromatography analysis (Dionex ICS 1100). The solution was freshly made each day from pure oxalic acid (Aldrich, 98%). No measurable $NH_3$ was found, suggesting that if a small amount of $NH_3$ was present, it was lower than the 10 ppt limit of detection.

In each experiment, the reaction of MSA with MA or TMA took place at the spoked inlets, while $NH_3$ was added either at one of the upstream rings or at the upstream spoke (spoke 1; Fig. 1a). In either case, all reactants were present simultaneously rather than reacting sequentially. Variable relative humidity (RH) inside the flow reactor was achieved by diverting part of the 13 L $min^{-1}$ flow of air (ring A) through a bubbler filled with Nanopure™ water (18.2 MΩ-cm; model 7146; Thermo Scientific, Barnstead) to yield RH < 3% to ~45-50% (corresponding to a water vapor concentration of ~$3 \times 10^{17}$ molecules $cm^{-3}$ at T = 296 K). The RH was monitored with an RH probe (model HMT338; Vaisala) located in the end cap of the flow reactor. The nanopure water was analyzed using the IC system described above to verify that it did not contain any $NH_3$ contamination, and the water trap was refilled with fresh water prior to each experiment. Particles were sampled through a moveable ¼" stainless steel tube mounted on the downstream end-cap of the flow tube to access reaction times ranging from 0.4 s to 5.3 s (MSA+MA system) and 0.3 s to 5.9 s (MSA+TMA system). Total particle number concentrations and size distributions were measured as a function of reaction time as described below.

**2. *Reactants***. Gas phase MSA was generated by passing 0.1 or 0.2 L $min^{-1}$ of dry clean air over the pure liquid (Sigma-Aldrich, ≥ 99%) which was maintained at room temperature in a glass trap. Periodically, the entire flow of MSA was directed into a 0.45 μm Durapore filter (Millex-HV) for 10 min. After sampling, the filter was extracted with 10 mL of nanopure water (each filter was extracted with 3 × 3 mL of nanopure water flow in the opposite direction to that used for sampling. This was followed by one additional extraction with 1 mL of nanopure water and the extracts were combined together to yield a 10 mL sample). The combined extracts were then analyzed by UPLC-ESI-MS/MS (Quattro Premier XE, Waters; MRM method following the *m/z* 95 => *m/z* 80 transition). Note that during the development of the method, a second extraction of the filter was performed and the second extract didn't show any traces of MSA, suggesting that one extraction is efficient at extracting all of the MSA collected. In some occasions, collection of the MSA exiting the trap was performed with two filters in series, but no MSA was measured in the second filter. Each measurement was done in triplicate.

Gas phase MA and TMA were generated by flowing dry clean purge air over commercially available permeation tubes containing the amines (VICI Metronics) that were maintained in a U-shaped glass trap at room temperature. The concentration of amine exiting the traps was determined periodically by ion chromatography (Dionex ICS 1100) after trapping the gases onto a custom-made cation-exchange resin, followed by three successive extractions with 10 mL of a 0.05 M oxalic acid aqueous solution flow in the opposite direction to that used for sampling.[116] The sum of the these three extractions was used for quantification, and each permeation tube measurement was done in triplicate. No quantifiable ammonia or other contaminants were detected for either permeation tube. The concentrations of the reactants

determined herein may be upper limits due to potential wall losses even after extensive conditioning.

***3. Particle measurements***. Total particle number concentrations ($N_{total}$, particles $cm^{-3}$) were measured at each reaction time using an ultrafine butanol-based condensation particle counter (CPC; model 3776; TSI; flow rate 1.5 L $min^{-1}$). Detectable particles are defined hereafter as those with a mobility diameter greater than 2.0 nm, which is the lowest diameter size the 3776 CPC can measure. The counting efficiency increases from 0% at 2.0 nm to 100% at 3.0 nm with a manufacturer-specified $d_{50}$ for this instrument of 2.5 nm defined as the diameter at which 50% of the particles are detected based on sucrose particles. Note that due to this limitation, the initial clusters nucleated from the present reactions were not detected, and it is only those that have grown to diameters > 2.0 nm that were measured; thus our measurements include nucleation and the first steps of growth. Parallel measurements using a combination of the CPC with a particle size magnifier (PSM; model A10; Airmodus)[148] leading to a lower diameter cut-off were also performed. As described in the SI, the operating conditions were set so that the $d_{10}$, $d_{50}$ and $d_{80}$ cut-offs (diameters at which 10%, 50%, and 80% of the particles are detected respectively) were 1.2 nm, 1.4 nm and 2.1 nm respectively, according to the manufacturer calibration using negatively charged ammonium sulfate particles. It is recognized that the true cut-off sizes for both the CPC and PSM strongly depends on the chemical composition of the particle sampled.[148-153] The cut-off sizes for the present MSA+amine particles are not known, thus the cut-offs defined for the reference compounds are applied here. Despite these distinctions, as reported in Figures S1 and S2 no significant differences were observed between the CPC and the combination PSM+CPC measurements for any of the systems studied. Thus, $N_{total}$ values are

reported hereafter for the CPC and SMPS as described below. Measurements with a HEPA filter at the beginning of each experiment were performed to ensure there was a zero background reading. When necessary (i. e. total counts > $3 \times 10^5$ particles $cm^{-3}$), the particle stream exiting the flow tube was diluted with purge air prior to entering the CPC.

Particle size distributions were also measured using a scanning mobility particle sizer (SMPS; TSI) equipped with a 0.071 cm impactor nozzle, a $^{210}Po$ bipolar charger (10 mCi; model 2021; NRD), an electrostatic classifier (model 3080; TSI), a nano differential mobility analyzer (nanoDMA; model 3085; TSI) and the 3776 model CPC. The SMPS was operated with the following settings: sheath air flow rate, 15 L $min^{-1}$ (recirculating mode); sample flow rate, 1.5 L $min^{-1}$. Under these conditions, the SMPS measured particles with mobility diameters ranging from 2 nm to 64 nm. To test for changes in the size distributions due to drying within the SMPS, some TMA experiments were carried out in which the sheath air was humidified to an RH of ~ 52% (apparatus shown in Fig. S3a). The MSA+TMA combination was chosen because it is the most hygroscopic of the two systems studied and is thus expected to be most sensitive to water.[154, 155] As shown in Figure S3b, the size distributions were very similar between measurements performed with humid sheath air (RH ~52%) versus those performed with dry recirculating air. No significant changes in the mobility geometric mean diameter (GMD) were observed when the sheath air was externally humidified (difference of only 2.9%). However, there was an apparent loss of the smallest particles with diameter < 20 nm (13% lower total number concentration for the humid runs compared to the dry recirculating sheath air runs). The use of an external dry air supply (Fig. S3c) produced a slightly stronger drying effect (difference in GMD of 4.1%). For simplicity, all measurements were carried out with dry recirculating sheath air (i.e. normal SMPS operating conditions) where the loss of the smallest particles is

minimized. To avoid potential reaction time bias, all particle measurements were performed after the system had reach steady state in the following order: 5.3-5.9 s, 2.9-3.1 s, 0.28-0.37 s, 1.6-1.7 s, 4.2-4.5 s and 5.3-5.9 s (the range represents the times for the two different flow tubes). Data collected from the SMPS were also used to estimate particle formation rates ($J_{>2.0nm}$) following the linear change in total particle number concentration ($N_{total}$) as:[2]

$$J_{>2.0nm} = \frac{\Delta N_{total}}{\Delta_t} \quad (1)$$

The determined $J_{>2.0nm}$ values represent apparent particle formation rates for each condition, as this treatment does not separate out processes such as the real nucleation rate of the smallest clusters (too small to see using our instrumentation), coagulation, scavenging or wall losses of the particles throughout the flow reactor (those processes might be more important at the largest concentrations observed, i.e. > $10^7$ particles $cm^{-3}$).

# Theoretical Methods

In this study, quantum calculations were carried out for small clusters of the precursor gases to provide theoretical insights into the formation and growth of particles in the MSA+amine ($\pm NH_3$) ($\pm H_2O$) systems. Thus, calculations of the energies, structures and partial charge distributions of relevant multi-component clusters were calculated using density functional methods. The effectiveness of this approach was previously demonstrated for clusters that include binary MSA-amine clusters and ternary MSA-amine-$H_2O$ clusters.[74, 82, 85, 119-121, 154, 156, 157] Similar approaches were previously used for acid:base particles containing $H_2SO_4$ with an amine or $NH_3$, and water.[30, 54, 55, 157-160]

Proton transfer to the amine was generally found for the lowest energy clusters, and this seems a key feature consistent with the interpretation of experimental observations.[119] One must

therefore employ quantum-chemical potentials that can adequately describe the acid+amine reaction, in addition to the hydrogen-bonding and Van der Waals interactions that are involved. The presence of both an amine and $NH_3$ in the multi-component clusters implies that competition for the MSA proton may take place. Accurate treatment of the proton transfer is thus essential.

All of the electronic structure calculations including geometry, frequency, and energy calculations were done using B3LYP variant[161-163] of density functional theory (DFT) with Grimme's dispersion correction.[164] The Dunning augmented double-ζ correlation-consistent basis set was employed. Note that basis set superposition errors were not considered here, based on the fact that the contribution of this effect was previously tested for similar systems,[165] and found to be small. In previous studies,[119] this method was tested against the MP2 method and the high level CCSD(T) method for the low-lying isomers of the binary MSA-MA cluster. The results show better-than-qualitative agreement between the three methods and support the adequacy of the B3LYP-D3 method for our purpose. There is evidence that DFT variants with hybrid functionals (including B3LYP) with Grimme's dispersion interaction corrections are reasonably successful methods in predicting the global minimum structures and the structures of low-lying conformers of involved water molecules.[166-169] Hence, B3LYP-D3 was chosen here as it offers a reasonable level of accuracy while being computationally efficient.

The initial structures of each system were randomly generated in an 8*8*8 Å cube with a minimum distance criterion of 1.8 Å between each molecule using the PACKMOL package.[170, 171] Using this program, 300 different initial structures were generated for each system, and energy minimization was carried out for these structures. To obtain Gibbs free energies (ΔG), the contribution from vibrational entropy was computed for each structure (at 298 K) and added in. Dissociation energies (De) and Gibbs free energies (ΔG) are calculated as followed: $D_e$ =

E(AB) - E(A) - E(B) and ΔG= G(AB) - G(A) - G(B). Note that the aug-cc-pVDZ basis may not always be sufficiently accurate for binding energies, but most often that basis set is adequate, and this is likely to be the case also here. All of the structures reported here were geometrically optimized at the level of B3LYP-D3/aug-cc-pVDZ. Note that no imaginary vibrational frequencies were observed in any of the cases presented, and all cases have the correct number of positive frequencies. In addition, zero-point energies (ZPE) were used to correct electronic energy values. Partial charges (denoted by δ) were calculated using natural bond orbital (NBO) analysis.[172, 173] All the calculations presented in this paper were performed using the Q-CHEM 4.3 program package.[174]

# Results and Discussions

### A. MSA + MA (± $NH_3$) Reaction

**1. Dry conditions.** Figure 2a shows the total number concentrations of particles ($N_{total}$) measured using the CPC for the MSA+MA system ([MSA] = $6.4 \times 10^{10}$ molecules $cm^{-3}$; [MA] = $6.1 \times 10^{10}$ molecules $cm^{-3}$), with or without $NH_3$ as a function of reaction time. In the absence of $NH_3$, nucleation of new particles is already extremely efficient with $N_{total}$ ranging from ~ 50 particles $cm^{-3}$ at 0.37 s to $(7.4 \pm 1.1) \times 10^4$ particles $cm^{-3}$ at 5.3 s. Upon the addition of $NH_3$ ($2.9 \times 10^{11}$ molecules $cm^{-3}$) to the MSA+MA system, the same trend is observed as a function of reaction time, with $N_{total}$ being systematically higher than that measured in the absence of $NH_3$. An enhancement factor (EF), defined as $N_{total}$ measured at 5.3 s in the presence of $NH_3$ (or $H_2O$) ratioed to that measured in the absence of $NH_3$ (or $H_2O$) was determined from this CPC dataset. The EF observed for MSA+MA (± $NH_3$) is modest, with a value of 1.6 ± 0.1 (Table 1). A separate series of measurements was performed under which MSA was in excess compared to

MA ([MSA]/[MA] ~2; [MSA] = 4.6 × $10^{10}$ molecules $cm^{-3}$; [MA] = 2.3 × $10^{10}$ molecules $cm^{-3}$), and again a modest enhancement was observed when $NH_3$ (1.1 × $10^{11}$ molecules $cm^{-3}$) was added to the flow reactor (average factor of 1.7 ± 0.8; Fig. S4). These enhancements may be lower limits as particles formed from the MSA+MA+$NH_3$ condition were approaching the limit for efficient CPC counting. Figure 2b presents the comparison between the mixed MSA+MA+$NH_3$ system and the respective MSA+MA and MSA+$NH_3$ systems ([MSA] = 6.4 × $10^{10}$ molecules $cm^{-3}$; [MA] = 0 or 6.1 × $10^{10}$ molecules $cm^{-3}$; [$NH_3$] = 0 or 2.9 × $10^{11}$ molecules $cm^{-3}$). It is evident that a modest synergy is present for this system, and the effect is simply not just additive: The MSA+$NH_3$ system is not efficient at forming particle on its own (only 5 particles $cm^{-3}$ were observed at 5.3 s, despite the large concentration of $NH_3$); however, the addition of $NH_3$ to the MSA+MA system enhances the total number of detectable particles by a factor of 2 compared to the MSA+MA binary system, as described above. It is likely that $NH_3$ grew the initial MSA+MA clusters that were too small to be detected to now be within the measurable range of our instrumentation (> 2 nm). These results thus show the first evidence for a synergism between MA and $NH_3$ in forming particles with MSA.

Experiments for which reaction time (5.3 s) and initial MSA concentration ([MSA] = 6.4 × $10^{10}$ molecules $cm^{-3}$) were fixed are illustrated in Figure S5. Figure S5a (filled red squares; no $NH_3$) shows that $N_{total}$ is correlated with the MA concentration, with few particles (< 40 particles $cm^{-3}$) observed for MA concentrations smaller than 1.7 × $10^{10}$ molecules $cm^{-3}$ (excess MSA conditions). For MA concentrations larger than 3.2 × $10^{10}$ molecules $cm^{-3}$, a significant particle number concentration is observed (> 5000 particles $cm^{-3}$). Previous studies[154, 156] predicted that MA can form tight nanosize $(MSA\text{-}MA)_4$ clusters with MSA that are extremely stable due to a substantial hydrogen bonding network, consistent with these observations. Indeed, quantum

calculations indicated that the dissociation energies ($D_e$ at 0 K as well as ΔG at 298 K) of this cluster into various smaller complexes were endothermic. In addition, dynamics showed that this cluster was stable for at least 100 ps at temperatures up to 500 K, well above atmospheric temperatures. Note that, on the other hand, the MSA+$NH_3$ system (Fig.2b and Fig. S5b; filled red triangles) itself is not as efficient at forming particles, with $N_{total}$ only reaching ~5 particles $cm^{-3}$ for $NH_3$ concentration of $2.9 \times 10^{11}$ molecules $cm^{-3}$ under dry conditions at 5.3 s.

Figure 2c and 2d show the size distributions for MSA+MA and MSA+MA+$NH_3$ conditions. Small particles with mobility diameters < 5 nm were observed for the MSA+MA system ([MSA] = $6.4 \times 10^{10}$ molecules $cm^{-3}$; [MA] = $6.1 \times 10^{10}$ molecules $cm^{-3}$), and in presence of $NH_3$ ($2.9 \times 10^{11}$ molecules $cm^{-3}$), $N_{total}$ increased but no significant growth was observed. The mobility geometric mean diameter (GMD) for particles measured at 5.3 s without $NH_3$ was 3.2 ± 0.1 nm, while it was 3.3 ± 0.1 nm in presence of $NH_3$ (Fig. S6a). In brief, $NH_3$ has only a modest impact on the MSA+MA system under dry conditions. Based on the SMPS data collected as a function of reaction time, particle formation rates ($J_{>2.0nm}$) were determined (Fig. S6b). The resulting values of $J_{> 2.0nm}$ for MSA+MA and MSA+MA+$NH_3$ systems are (2.2 ± 0.4) $\times 10^4$ particles $cm^{-3}$ $s^{-1}$ and (8.0 ± 0.7) $\times 10^4$ particles $cm^{-3}$ $s^{-1}$ respectively.

**2. In the presence of water vapor.** Figure 3a shows $N_{total}$ values measured using the CPC for the MSA+MA+$H_2O$ system at ~45-50% RH with and without $NH_3$ as a function of reaction time ([MSA] = $6.4 \times 10^{10}$ molecules $cm^{-3}$; [MA] = $6.1 \times 10^{10}$ molecules $cm^{-3}$). Comparing Figure 2a (MSA+MA; red trace) and Figure 3a (MSA+MA+$H_2O$; orange trace), it is apparent that the addition of water vapor alone (without added $NH_3$) increases the total number of particles detected, leading to $N_{total}$ values of ~$10^7$ particles $cm^{-3}$ at 5.3 s (enhancement factor of 63 ± 1.3

compared to the dry case; Table 1). The size distribution with water present (Fig. 3c) showed larger particles than the corresponding dry system with GMD of 4.7 ± 0.07 nm at 0.37 s and 6.1 ± 0.1 nm at 5.3 s (Fig. S7), compared to ~ 3 nm for the dry system. This is consistent with a previous study[154] where a large enhancement in particle formation and growth was observed for MSA+MA when water was added *simultaneously with* MSA and MA (measurements performed at t = 13.9 s). In contrast, *subsequently* exposing initially dry particles from MSA+MA reaction to water vapor did not enhance particle formation or significantly grow them (in this case, the MSA and MA reacted for 8.2 s before interacting with water vapor for an additional 5.7 s to reach the sampling line). A proposed molecular explanation based on quantum chemical calculations[154] is that in the former case, water molecules incorporated into the cluster can act as the hydrogen bond donor and acceptor for the initial cluster to grow, whereas in the latter case, the tight MSA-MA ion pair system is too stable to be disrupted by water molecules. By comparison, MSA+$H_2O$ itself only formed about 20 particles $cm^{-3}$ throughout the flow reactor at ~45-50% RH (light blue trace in Fig. 3a). Figure S5a shows near identical $N_{total}$ values for the MSA+MA+$H_2O$ reaction at both ~18% RH and 45-50% RH.

In the presence of $NH_3$ (Fig. 3a; $[NH_3] = 2.9 \times 10^{11}$ molecules $cm^{-3}$) no apparent enhancement is observed. As seen in Figures 3c-d and S7a, the particles did not grow upon addition of $NH_3$, and $N_{total}$ is similar at 5.3 s (Fig. S7b). Either with or without $NH_3$, a plateau in the number concentrations is observed after 1.6 s, suggesting that particles form quickly (0-1.6 s) and then continue to slowly grow by condensation of vapors. This highlights the role of water in the growth of particles when present as MSA and MA are reacting, consistent with our earlier studies.[73, 85, 154]

It is noteworthy that the MSA+$NH_3$+$H_2O$ reaction where [$NH_3$] = 2.9 × $10^{11}$ molecules $cm^{-3}$ (with [MSA] = 6.4 × $10^{10}$ molecules $cm^{-3}$) actually produces a similar number of particles to the MSA+MA+$H_2O$ reaction (Fig. S5; [MSA] = 6.4 × $10^{10}$ molecules $cm^{-3}$; [MA] = 6.1 × $10^{10}$ molecules $cm^{-3}$). The effect of $NH_3$ (2.8 × $10^{11}$ molecules $cm^{-3}$) on the MSA+MA+$H_2O$ system is not additive (Fig. 3b and Fig. S8), and little enhancement in $N_{total}$ is observed. This suggests that most of the MSA is tied up with MA and water, and little is left in its 'free' form to interact with $NH_3$. It also suggests that $NH_3$ does not disrupt the MSA-MA-$H_2O$ clusters. Chemical composition measurements on these sub-20 nm particles would confirm the presence or absence of $NH_3$ in these particles, but was outside of the scope of this paper.

From the SMPS data collected as a function of time (Fig. 3c and d), particle formation rates ($J_{>2.0nm}$) were estimated to be 1.4 × $10^7$ particles $cm^{-3}$ $s^{-1}$ (no $NH_3$) and 1.5 × $10^7$ particles $cm^{-3}$ $s^{-1}$ (with $NH_3$) (Fig. S7b), which are much higher than the dry case, highlighting the importance of water in this system.

**3. Insights from theoretical calculations.** The structures of the most stable MSA-MA clusters with and without $NH_3$ are shown in Figure 4. The corresponding energies for dissociation to the monomers, and corresponding Gibbs free energies are listed in Table 2. First, for the 1MSA-1MA (Fig. 4a) and 2MSA-2MA (Fig. 4c) clusters without $NH_3$, the most stable structures involve a proton transfer (δ = 0.83 - 0.85) from the acid to the base forming an ion pair, consistent with our previous studies.[85, 119]

For the 1MSA-1MA-1$NH_3$ (Fig. 4b) and 2MSA-2MA-2$NH_3$ (Fig. 4d) clusters, the key skeletons of the clusters do not change significantly compared to those without $NH_3$, and the positive charges on $NH_3$ (δ = 0.06) mean that $NH_3$ makes only a small contribution to charge

transfer from MSA. Note that extensive sampling of the initial configurations was carried out using the PACKMOL code. In principle, this approach should reveal significant changes in structural parameters, if such changes indeed occur. The dominant charge acceptor ($\delta$ = 0.79 - 0.81) remains the stronger base, MA (gas phase basicity, GB, is 864.5 kJ $mol^{-1}$ for MA versus 819.0 kJ $mol^{-1}$ for $NH_3$).[175] When compared to those without $NH_3$, the dissociation energies of clusters with $NH_3$ increase from 15 to 29 kcal/mol for the 1MSA-1MA-1$NH_3$ cluster and from 68 to 92 kcal/mol for the 2MSA-2MA-2$NH_3$ cluster (Table 2). The corresponding Gibbs free energies increase from 4 to 10 kcal/mol, and from 35 to 40 kcal/mol, respectively. The fact that the energies are systematically higher in the presence of $NH_3$ indicates that the species are more strongly bound to each other within the cluster and that the cluster, if formed, is more thermodynamically stable with respect to dissociation compared to that without $NH_3$. In brief, the main effect of $NH_3$ in the MSA+MA system is to provide hydrogen bonds to MSA and MA, forming a more stable closed structure. Furthermore, although the skeletons of clusters with and without $NH_3$ do not change significantly, the addition of $NH_3$ provides extra hydrogen bond opportunities to incoming gas phase molecules where they can potentially attach to grow the initial clusters to detectable particles. These calculations are consistent with the experimental findings where only a modest enhancement in particle number concentration was observed upon addition of $NH_3$.

The structures of the 1MSA-1MA-1$H_2O$ and 2MSA-2MA-2$H_2O$ clusters with and without $NH_3$ are shown in Figure 4e-4h, and the corresponding dissociation energies and Gibbs free energies are in Table 2. In all these clusters, the proton is always transferred from MSA to MA whether or not $NH_3$ is present, similar to the dry conditions. For comparison, Wang et al.[114] recently reported quantum calculations in which all the 1$H_2SO_4$-1MA-1$NH_3$ clusters investigated

with various numbers of water molecules systematically show proton transfer from the acid to MA. For the MSA+MA system presented here, the role of $NH_3$ is analogous to that of $H_2O$, as both can form more hydrogen bonds within the clusters, stabilizing their structures compared to that of the corresponding MSA+MA system (Table 2). Both also have the capability of hydrogen bonding to incoming molecules. For example, the 1MSA-1MA-1$H_2O$ (Fig. 4e) exhibits one free -OH on the water molecule, while the 2MSA-2MA-2$H_2O$ (Fig. 4g) exhibits two hydrogen bond acceptor sites on the water oxygens. Similarly, for the 1MSA-1MA-1$NH_3$ cluster (Fig. 4b), the cluster has two potential hydrogen bond donor sites located on the $NH_3$, while for the 2MSA-2MA-2$NH_3$ cluster (Fig. 4d) there is one on each ammonia. From the viewpoint of partial charge, $NH_3$ has only a small contribution ($\delta = 0.06$), and $H_2O$ has a minor contribution to the separation of charges ($\delta = 0.00 - 0.03$). It is interesting to note that the charge distribution on the water decreases upon addition of $NH_3$ to the 2MSA-2MA-2$H_2O$ complex.

**B. MSA + TMA (± $NH_3$) System**

**1. Dry conditions.** Figure 5a presents $N_{total}$ values for the MSA+TMA reaction system ([MSA] = $7.9 \times 10^{10}$ molecules $cm^{-3}$; [TMA] = $5.0 \times 10^{10}$ molecules $cm^{-3}$), in the presence or absence of $NH_3$, as a function of reaction time. Under dry conditions, the MSA+TMA reaction is not very effective at forming particles, where only 2 particles $cm^3$ are detected at 5.9 s. However, as seen in Figure 5a-b, adding $NH_3$ at about half the concentration of TMA ([$NH_3$] = $2.2 \times 10^{10}$ molecules $cm^{-3}$) produced an immediate enhancement by four orders of magnitude in $N_{total}$ (Table 1). Figure 5c shows the corresponding size distributions when $NH_3$ is present (too few particles above 2.0 nm were generated in the MSA+TMA system alone to be measured by SMPS). In addition to the increase in the particle number concentration, the particles are

observed to grow over time, with the GMD increasing from 4.0 ± 0.1 nm at 1.7 s to 5.4 ± 0.1 nm at 5.9 s (Fig S9a). The particle formation rate ($J_{>2.0nm}$) was estimated based on the SMPS data to be (7.6 ± 0.5) × $10^3$ particles $cm^{-3}$ $s^{-1}$ under these conditions (Fig. S9b).

A separate set of experiments was carried out at various concentrations of $NH_3$ (0 to 10 × $10^{10}$ molecules $cm^{-3}$) while keeping MSA and TMA constant ([MSA] = 6.4 × $10^{10}$ molecules $cm^{-3}$; [TMA] = 4.8 × $10^{10}$ molecules $cm^{-3}$). As seen in Figure 6a, $N_{total}$ increased with the concentration of $NH_3$. Enhancement factors were estimated from this dataset and are shown as a function of the $NH_3$ concentration in Figure 6b. At $NH_3$ concentrations < 1.4 × $10^{10}$ molecules $cm^{-3}$ (0.55 ppb), some enhancement is already observed (EF < 100), but at [$NH_3$] >1.9 × $10^{10}$ molecules $cm^{-3}$ (> 0.78 ppb), the enhancement factor becomes 3 to 6 orders of magnitude, with EF reaching ~$10^6$ at [$NH_3$] = 10 × $10^{10}$ molecules $cm^{-3}$ (4.1 ppb). Thus, the presence of $NH_3$ even at relatively small concentrations drastically enhances NPF in the MSA+TMA system, which is not very efficient in forming particles on its own. Particle nucleation rates ($J_{>2.0nm}$) were estimated from the CPC data (no SMPS measurements were performed for this dataset) and ranged between 1.3 particles $cm^{-3}$ $s^{-1}$ to 3.2 × $10^4$ particles $cm^{-3}$ $s^{-1}$ for $NH_3$ concentrations of (0.96-10) × $10^{10}$ particles $cm^{-3}$ (Fig. S10). In short, although the MSA+TMA system is not very efficient at producing particles on its own, adding $NH_3$ can give particle nucleation rates similar to that of the MSA+MA system.

The above MSA+TMA experiments were performed with excess MSA ([MSA]/[TMA] ~1.6). Additional experiments were performed at various [MSA]/[TMA] ratios (Fig S11). In these, a large enhancement upon addition of $NH_3$ was systematically observed for each condition, and for an equal concentration of MSA and TMA ([MSA] = [TMA] = 6.4 × $10^{10}$ molecules $cm^{-3}$), the enhancement was still about 2 orders of magnitude under dry conditions.

Note that the enhancement is not simply due to increase of condensing vapors. Indeed, as illustrated in Fig. S11, for a fixed MSA concentration of $6.4 \times 10^{10}$ molecules $cm^{-3}$ and an equivalent total base concentration, i.e. ~$3 \times 10^{10}$ molecules $cm^{-3}$, an enhancement is clearly visible when comparing to the MSA+TMA reaction alone (middle red bar; [total base] = [TMA] = $3 \times 10^{10}$ molecules $cm^{-3}$; no $NH_3$), $N_{total}$ observed at 5.3 s is $1.7 \pm 0.3$ particles $cm^{-3}$, whereas it is $216 \pm 82$ particles $cm^{-3}$ when $NH_3$ is present (keeping [total base] ~$3 \times 10^{10}$ molecules $cm^{-3}$; [TMA] = $1.4 \times 10^{10}$ molecules $cm^{-3}$; [$NH_3$] = $1.8 \times 10^{10}$ molecules $cm^{-3}$). For comparison, the total particle number concentration observed in the case of MSA+$NH_3$ alone ([$NH_3$] = [total base] = (2.4-3.8) $\times 10^{10}$ molecules $cm^{-3}$) is only 0.01-0.02 particles $cm^{-3}$ (Fig. S5).

**2. In the presence of water vapor.** Without $NH_3$ but in the presence of ~45-50% RH (as seen from the comparison between the red trace in Figure 5a and the orange trace in Figure 7a), the addition of water to the MSA+TMA system ([MSA] = $7.9 \times 10^{10}$ molecules $cm^{-3}$; [TMA] = $5.0 \times 10^{10}$ molecules $cm^{-3}$) enhances new particle formation compared to the dry case (EF = $(1.8 \pm 0.4) \times 10^2$; Table 1**)**. However, while $N_{total}$ remains relatively small ($(4.1 \pm 0.1) \times 10^2$ molecules $cm^{-3}$ at 5.9 s), the particles are much larger, with a GMD of $20 \pm 0.5$ nm, compared to 4-5 nm for the dry case. This is also different from the MSA+MA reaction system where particles only grew to about 6 nm upon addition of water.

Upon addition of $NH_3$ ($2.2 \times 10^{10}$ molecules $cm^{-3}$) to the MSA+TMA+$H_2O$ system, there is a clear enhancement in particle number concentration (Fig. 7a-b); however, as displayed in Table 1, the EF is less than that in the dry case (EF = $(2.6 \pm 0.5) \times 10^2$ under humid conditions, compared to 4 to 6 orders of magnitude under dry conditions). In this case, the particle mobility GMD for MSA+TMA is centered around $17.9 \pm 0.4$ nm, which is slightly smaller than that in the

absence of $NH_3$. This suggests that while water is responsible for the growth of the particles, the main effect of $NH_3$ is to enhance nucleation to form new particles. Note that a lower, but still significant enhancement was observed for experiments performed under equivalent MSA and TMA conditions ([MSA] = [TMA] = $6.4 \times 10^{10}$ molecules $cm^{-3}$; RH ~45-50%), with EF = 19 ± 11 in this case upon addition of $NH_3$ ($1.8 \times 10^{10}$ molecules $cm^{-3}$) (Fig. S12).

From the size distributions measured for MSA+TMA+$H_2O$ (Fig. 7c and d; [MSA] = $7.9 \times 10^{10}$ molecules $cm^{-3}$; [TMA] = $5.0 \times 10^{10}$ molecules $cm^{-3}$; RH ~45-50%), particle formation rates ($J_{>2.0nm}$) were determined (Fig. S13) to be $(1.7 \pm 0.06) \times 10^2$ particles $cm^{-3}$ $s^{-1}$ (no $NH_3$) and $(6.5 \pm 0.03) \times 10^4$ particles $cm^{-3}$ $s^{-1}$ (with $NH_3$; [$NH_3$] = $2.2 \times 10^{10}$ molecules $cm^{-3}$). The corresponding $J_{>2.0nm}$ value for MSA+TMA+$NH_3$ under dry conditions and equivalent concentrations of the reactants (Fig. S9) was only $7.6 \times 10^3$ particles $cm^{-3}$ $s^{-1}$, suggesting that the presence of water greatly enhanced particle formation. In addition, the quaternary system MSA+TMA+$H_2O$+$NH_3$ appears to be as efficient at forming particles as the ternary MSA+MA+$NH_3$ reaction system (dry conditions; [MSA] = $6.4 \times 10^{10}$ molecules $cm^{-3}$; [MA] = $6.1 \times 10^{10}$ molecules $cm^{-3}$; [$NH_3$] = $2.9 \times 10^{11}$ molecules $cm^{-3}$). However, the particles exhibit larger diameters (GMD = 17 nm for the quaternary MSA+TMA+$H_2O$+$NH_3$ system versus GMD ~3 nm for the ternary MSA+MA+$NH_3$ system).

**3. Theory Calculations.** The structures of the most stable MSA-TMA clusters with and without $NH_3$ are presented in Figure 8 and the corresponding dissociation energies and Gibbs free energies are in Table 2. In the case of the 1MSA-1TMA (Fig. 8a) and 2MSA-2TMA (Fig. 8c) clusters without $NH_3$, the most stable structures involve a proton transfer ($\delta$ = 0.83-0.86) between MSA and TMA forming an ion pair, consistent with our previous studies.[74, 82, 85] Note

that for the 2MSA-2TMA cluster, there are no hydrogen bonds between the two MSA-TMA ion pairs, which is a distinct difference from the MSA-MA clusters presented above. The 2MSA-2TMA cluster is bound by Van der Waals interactions, of which the largest contribution is dipole-dipole interaction. Two dissociation pathways were considered for this cluster: 2MSA-2TMA => 2 MSA + 2 TMA and 2MSA-2TMA => 2 (MSA-TMA). The corresponding Gibbs free energies for the two pathways at T = 298 K are 30 kcal/mol and 12 kcal/mol, respectively. The free energy changes are positive in both indicating that the dissociation reactions are endothermic, and the cluster, if it is formed, is thermodynamically stable with respect to dissociation. However due to the absence of free -NH groups on TMA, the 2MSA-2TMA cluster does not have any potential hydrogen opportunities for incoming molecules to attach to this cluster. This is consistent with the experimental observations that the MSA+TMA system is not very efficient at forming detectable particles.

The role of $NH_3$ in the 1MSA-1TMA-1$NH_3$ cluster (Fig. 8b) is similar to that observed in the MSA+MA system, where $NH_3$ simply attaches to the ion pair with minimal contribution to the separation of charges ($\delta = 0.01$) and the proton transfer remains between MSA and TMA ($\delta = 0.83$). However, for the 2MSA-2TMA-2$NH_3$ cluster (Fig. 8d), the structure surprisingly shows a significant change. In this case, the proton is transferred from MSA to $NH_3$ instead of to TMA. This is also seen in the partial charge distribution on $NH_3$ ($\delta = 0.77$), showing that $NH_3$ now becomes the dominant acceptor. Similar observations were recently reported for $H_2SO_4$-dimethylamine-$NH_3$ clusters,[112] where $NH_3$ formed more intermolecular interactions than dimethylamine within the cluster and it was the species that was accepting the proton from the acid, although dimethylamine is a stronger base (gas phase basicity, GB = 896.5 kJ $mol^{-1}$).[175]

When $NH_3$ is present, the 2MSA-2TMA-2$NH_3$ cluster (Fig. 8d) possesses a closed ring structure, where two $NH_3$ and two MSA form a core and TMA is bound on the outside of this core, unlike the 2MSA-2TMA open structure cluster (Fig. 8c). Although TMA is a much stronger base (gas phase basicity, GB = 918.1 kJ $mol^{-1}$),[175] $NH_3$ (GB = 819.0 kJ $mol^{-1}$)[175] can form more hydrogen bonds, leading to a much more stable structure. Indeed, the dissociation energy increases from 63 to 89 kcal/mol, and the corresponding Gibbs free energy increases from 30 to 35 kcal/mol (Table 2). In addition, the presence of $NH_4^+$ in the cluster structure offers hydrogen bonding opportunities for incoming gases to potentially attach to the cluster and grow it to detectable sizes. This remarkable shift in charge distribution, stability and structure of the clusters parallels the large enhancement observed in the experiments, where the presence of $1.0 \times 10^{11}$ $NH_3$ molecules $cm^{-3}$ (Fig. 6) in the dry MSA+TMA reaction system induced enhancements in particle formation by up to six orders of magnitude.

Proton transfer occurs between MSA and TMA in the 1MSA-1TMA-1$H_2O$ (Fig. 8e) and 2MSA-2TMA-2$H_2O$ clusters (Fig. 8g), as well as for the 1MSA-1TMA-1$H_2O$-1$NH_3$ cluster (Fig. 8f). Note that, in the 2MSA-2TMA-2$H_2O$ cluster (Fig. 8g), $H_2O$ acts as a bridge between the ion pairs, increasing the stability of the cluster. In the 2MSA-2TMA-2$NH_3$-2$H_2O$ cluster (Fig. 8h) involving $NH_3$, ammonia is the dominant proton acceptor ($\delta = 0.78$) as observed in the dry system, and TMA and $H_2O$ connect with the other species through hydrogen bonds. This is also consistent with the experiments, although a much smaller enhancement was observed in the presence of water vapor (~45-50% RH) compared to the dry case.

## C. Comparison of the addition of $NH_3$ versus the addition of $H_2O$

For the MSA+MA reaction system, which is already very efficient in forming small particles under dry conditions, the addition of $NH_3$ induces only a modest enhancement. However, water promotes growth, which enhances the concentrations of particles.

For the MSA+TMA system, a small amount of $NH_3$ is far more effective in enhancing new particle formation than the larger atmospherically relevant amounts of water. Indeed, the addition of $NH_3$ ($2.2 \times 10^{10}$ molecules $cm^{-3}$) to the MSA+TMA reaction system gave a large increase in particle formation of four orders of magnitude, compared to an increase of $(1.8 \pm 0.4) \times 10^2$ (Table 1) upon the addition of water at much higher concentrations, ~$3 \times 10^{17}$ molecules $cm^{-3}$ (equivalent to ~45-50% RH). The presence of $NH_3$ promotes the formation of a strong hydrogen bonding network which enables the formation of stable clusters. In addition, $NH_3$ replaces the strong base TMA as the main proton acceptor in the dimer systems. On the other hand, water provides hydrogen bonding opportunities that help to grow the particles. This is seen in the much larger diameter observed upon the addition of water, compared to the respective dry cases (with and without $NH_3$).

It is important to note that the reverse addition (i.e. adding small amount of TMA to the binary MSA+$NH_3$ system) is also of atmospheric relevance. On its own, the binary dry system MSA+$NH_3$, even at high concentrations of $NH_3$ (up to $2.8 \times 10^{11}$ molecules $cm^{-3}$), is not effective at forming particles (only ~5 particles $cm^{-3}$ observed at t = 5.3 s; Fig. S5; [MSA] = $6.4 \times 10^{10}$ molecules $cm^{-3}$). However, with both TMA ($4.8 \times 10^{10}$ molecules $cm^{-3}$) and $NH_3$ ($1.0 \times 10^{11}$ molecules $cm^{-3}$) present, $N_{total}$ increased by $(2.1 \pm 0.5) \times 10^4$ (Fig. S14).

**D. Atmospheric Implications**

In air, gas phase $H_2SO_4$ is generally recognized as the main driver for new particle formation. However, increasing numbers of laboratory studies[73, 74, 82-85] and field measurements[8, 11, 16, 101, 176-178] suggest that MSA may also contribute. For example, we determined in this study apparent particle formation rates that suggest that the MSA-MA/TMA-$NH_3$ multi-component system may be extremely efficient at forming particles; however, direct application of these rates to atmospheric conditions is not straightforward. Nevertheless, evidence from field measurements show that MSA may be a key player in particle formation and growth. For example, MSA was measured in nucleation-mode particles above a forest canopy in Hyytiälä, Finland[8, 11] Recent measurements from the Arctic[176, 177] indicated a strong correlation between summertime particle number concentrations and particulate MSA concentrations, a period during which sulfate content is lower. Furthermore, Kerminen et al.[101] showed that MSA was enhanced compared to nss-$SO_4$ in sub-100 nm particles collected in the Finnish Arctic.

In addition, the role of MSA in NPF is expected to increase in the future, as anthropogenic $SO_2$ declines worldwide.[86-91] In addition, polar sea-ice is melting at an increasing rate. This is altering the marine ecosystem, providing more open ocean surface, and as consequence, higher emissions of DMS (precursor to MSA). For example, Sharma et al.[179] reported higher MSA concentrations in particles as the seasonal ice cover was reduced throughout the Arctic region.

While there are not many simultaneous co-located measurements of MSA and amines, there is growing evidence that ambient particles containing MSA also contain significant amounts of aminium and/or aminium ions. .[8, 11, 16, 100, 137-141] For example, Kollner et al.[139] reported the presence of trimethylamine, $NH_3$ and MSA in the same particles in the Canadian Arctic, while Muller et al.[141] reported the co-existence of MSA with MA and $NH_3$ (along with

dimethylamine and diethylamine) from measurements performed in a marine environment at Cape Verde. In more polluted regions, such as agriculturally intensive areas where both ammonia and amines are present in relatively high concentrations,[115-117, 131, 180] the chemistry highlighted in the present study may also play a role. Thus, MSA and its precursor (DMS) have been previously measured in presence of amines and ammonia in agricultural settings[88, 181, 182] For example, Fielberg et al.,[181] measured DMS and TMA from an experimental pig production farm in Denmark, and Sorooshian et al.[183] reported high concentrations of MSA in particles collected near a cattle feedlot in California (35 ng $m^{-3}$).

In short, MSA, amines and $NH_3$ co-exist in various environments in the atmosphere from remote to polluted locations. The results presented here suggest that when combined, those species may have a significant role in particle formation and growth, but clearly there is a need for more parallel measurements of those species as well as the composition of the smallest particles to fully assess the importance of this chemistry in air.

## Conclusions

The present study demonstrates that ammonia systematically enhances particle formation from the reaction of MSA with MA and TMA to various degrees depending on the amine. For MSA+MA, the addition of $[NH_3] = 2.9 \times 10^{11}$ molecules $cm^{-3}$ gives only a small enhancement (EF = 1.6 ± 0.1, dry conditions; little to no enhancement in the presence of water vapor). On the other hand, addition of much smaller $NH_3$ concentrations ($2.2 \times 10^{10}$ molecules $cm^{-3}$) to the MSA+TMA binary reaction system has a much larger impact, with EF up to $10^4$ under dry conditions, but a smaller enhancement under humid conditions (EF = $(2.6 \pm 0.5) \times 10^2$). Most

importantly, although NPF from the MSA+TMA system is not efficient on its own, upon addition of $NH_3$ this system becomes competitive with the highly effective MSA+MA system.

One of the highlights of this study is that for the MSA+TMA reaction system, the addition of only ppb levels of $NH_3$ produces a much larger impact on NPF than the addition of much higher concentrations of water (~45-50% RH corresponding to ~12,000 ppm). While $NH_3$ stabilizes the clusters by providing a network of hydrogen bonds, leading to stable detectable nuclei, water bridges ion pairs and provides hydrogen-bonding opportunities to grow the initial cluster to diameters of 17-20 nm. In the case of MSA+TMA, surprisingly, $NH_3$ even becomes the acceptor for the proton from MSA, despite its weaker gas phase basicity compared to TMA.

The powerful combination of experimental results and quantum chemical calculations highlights the molecular basis for synergy occurring in the acid-base reactions involving MSA with MA or TMA in the presence of $NH_3$. These results are of particular importance as $NH_3$ is ubiquitous in air, and is almost always simultaneously present with amines both outdoors and indoors.[115, 132]

## Conflicts of Interests

There are no conflicts of interests to declare.

## Acknowledgements

The authors are grateful to the National Science Foundation (Grants No. 1443140, 1337080 and 1928252) for supporting this research.

# Electronic Supplementary Information

Online Supplementary Information for this article can be accessed on the publisher's website.

**Table 1.** Total particle number concentration enhancement factors (EF) for each MSA+amine reaction[a]

| Reference case | [MSA] (molecules $cm^{-3}$) | [$H_2O$] (molecules $cm^{-3}$) | Enhancement factor ($EF_{CPC}$) + $H_2O$[b] | Enhancement factor ($EF_{CPC}$) + $NH_3$ | Enhancement factor ($EF_{SMPS}$) + $H_2O$[b] | Enhancement factor ($EF_{SMPS}$) + $NH_3$ |
|---|---|---|---|---|---|---|
| Methylamine ([MA] = $6.1 \times 10^{10}$ molecules $cm^{-3}$) | | | | | | |
| MSA+MA | $6.4 \times 10^{10}$ | - | 63 ± 1.3 | 1.6 ± 0.1[c] | $(2.0 \pm 0.4) \times 10^2$ | 3.7 ± 0.7[c] |
| MSA+MA+$H_2O$ | $6.4 \times 10^{10}$ | ~$3 \times 10^{17}$ | - | 1.1 ± 0.02[c] | - | 0.86 ± 0.1[c] |
| Trimethylamine ([TMA] = $5.0 \times 10^{10}$ molecules $cm^{-3}$) | | | | | | |
| MSA+TMA | $7.9 \times 10^{10}$ | - | $(1.8 \pm 0.4) \times 10^2$ | $(1.1 \pm 0.3) \times 10^4$ [d, e] | n/a[f] | n/a[f] |
| MSA+TMA+$H_2O$ | $7.9 \times 10^{10}$ | ~$3 \times 10^{17}$ | - | $(2.6 \pm 0.5) \times 10^2$ [d] | - | $(3.8 \pm 0.7) \times 10^2$ [d] |

[a]From data in Figures 1 and 2 (MA) and Figures 5 and 7 (TMA).
[b]Experiments performed at ~45-50% RH corresponding to ~$3 \times 10^{17}$ molecules $cm^{-3}$
[c]$[NH_3] = 2.9 \times 10^{11}$ molecules $cm^{-3}$
[d]$[NH_3] = 2.2 \times 10^{10}$ molecules $cm^{-3}$
[e]Enhancement factors up to $1.1 \times 10^6$ were observed for $[NH_3] = 1.0 \times 10^{11}$ molecules $cm^{-3}$ (see Fig. 5; [MSA] = $6.4 \times 10^{10}$ molecules $cm^{-3}$; [TMA] = $4.8 \times 10^{10}$ molecules $cm^{-3}$)
[f]The MSA+TMA reaction did not generate enough particles to be observable by the SMPS.

**Table 2.** Dissociation energies with zero-point energy correction ($D_e$) and Gibbs free energies at 298 K ($\Delta G$) at the level of B3LYP-D3/aug-cc-pVDZ. A positive value corresponds to an endothermic process. B represents the alkyl amines. B = base (MA or TMA).

| Dissociation Reaction | $D_e$ (kcal/mol) | | $\Delta G$ (kcal/mol) | |
|---|---|---|---|---|
| | MA | TMA | MA | TMA |
| MSA-B → MSA + B | 15 | 20 | 4 | 9 |
| MSA-B-$NH_3$ → MSA + B + $NH_3$ | 29 | 29 | 10 | 10 |
| 2MSA-2B → 2MSA + 2B | 68 | 63 | 35 | 30 |
| 2MSA-2B-2$NH_3$ → 2MSA + 2B + 2$NH_3$ | 92 | 89 | 40 | 35 |
| MSA-B-$H_2O$ → MSA + B + $H_2O$ | 30 | 32 | 10 | 9 |
| MSA-B-$NH_3$-$H_2O$ → MSA + B + $NH_3$ + $H_2O$ | 43 | 40 | 15 | 11 |
| 2MSA-2B-2$H_2O$ → 2MSA + 2B + 2$H_2O$ | 95 | 80 | 42 | 27 |
| 2MSA-2B-2$H_2O$-2$NH_3$ → 2MSA + 2B + 2$H_2O$ + 2$NH_3$ | 112 | 113 | 42 | 41 |

# Figure Captions

**Figure 1.** Schematics of the flow reactors used to investigate new particle formation from (a) the MSA+MA (±$NH_3$) reaction and (b) the MSA+TMA (±$NH_3$) reaction. The diagrams are adapted from ref. 73 and 147.

**Figure 2.** (a) Total particle number concentrations ($N_{total}$) from MSA+MA and MSA+MA+$NH_3$ reactions as a function of reaction time measured using the CPC (dry conditions). Each data point corresponds to the average $N_{total}$ measured over a 5-min scan (error bars correspond to 1 standard deviation). (b) Comparison of $N_{total}$ values measured at 5.3 s for MSA+$NH_3$, MSA+MA and MSA+MA+$NH_3$. Size distributions measured using the SMPS are presented in (c) for the MSA+MA and (d) for the MSA+MA+$NH_3$ reactions respectively. Each size distribution is given in light colors with a log normal fit to guide the eye (each distribution corresponds to an average from five successive scans, except for reaction time 5.3 s where ten scans were averaged instead (standard deviation are not shown for clarity)). Concentrations of reactants for all panels are [MSA] = $6.4 \times 10^{10}$ molecules $cm^{-3}$; [MA] = 0 or $6.1 \times 10^{10}$ molecules $cm^{-3}$; [$NH_3$] = 0 or $2.9 \times 10^{11}$ molecules $cm^{-3}$.

**Figure 3.** (a) Total particle number concentrations ($N_{total}$) from MSA+$H_2O$, MSA+MA+$H_2O$ and MSA+MA+$H_2O$+$NH_3$ reactions as a function of reaction time measured using the CPC (RH ~45-50%). Each data point corresponds to the average $N_{total}$ measured over a 5-min scan (error bars correspond to 1 standard deviation). (b) Comparison of $N_{total}$ values measured at 5.3 s for MSA+$H_2O$+$NH_3$, MSA+$H_2O$+MA and MSA+$H_2O$+MA+$NH_3$. Size distributions measured using the SMPS are presented in (c) for the MSA+MA+$H_2O$ and (d) for the MSA+MA+$H_2O$+$NH_3$ reactions respectively. Each size distribution is given in light colors with a log normal fit to guide the eye (each distribution corresponds to an average from five successive scans, except for reaction time 5.3 s where ten scans were averaged instead (the standard deviation is not shown for clarity)). Concentrations of reactants for all panels are [MSA] = $6.4 \times 10^{10}$ molecules $cm^{-3}$; [MA] = 0 or $6.1 \times 10^{10}$ molecules $cm^{-3}$; [$NH_3$] = 0 or $2.9 \times 10^{11}$ molecules $cm^{-3}$.

**Figure 4.** Structures with distances (in angstroms) and partial charges δ (in atomic units) of the most stable structures of complexes composed of MSA, MA, $NH_3$ and $H_2O$ at the level of B3LYP-D3/aug-cc-pVDZ.

**Figure 5.** (a) Total particle number concentrations ($N_{total}$) from MSA+TMA and MSA+TMA+$NH_3$ reaction systems as a function of reaction time measured using the CPC (dry conditions). Each data point corresponds to the average $N_{total}$ measured over a 5-min scan (error bars correspond to 1 standard deviation). (b) Comparison of $N_{total}$ values measured at 5.9 s for MSA+$NH_3$, MSA+TMA and MSA+TMA+$NH_3$. (c) Size distribution for the MSA+TMA+$NH_3$ reaction. (The MSA+TMA reaction didn't generate enough particles to be observable by the SMPS). Each size distribution is given in light colors with a log normal fit to guide the eye (each

distribution corresponds to an average from five successive scans, except for reaction time 5.9 s where ten scans were averaged (standard deviation are not shown for clarity)). Concentrations of reactants for all panels are [MSA] = $7.9 \times 10^{10}$ molecules $cm^{-3}$; [TMA] = 0 or $5.0 \times 10^{10}$ molecules $cm^{-3}$; [$NH_3$] = 0 or $2.2 \times 10^{10}$ molecules $cm^{-3}$. Note that at 0.28 s, particles (> 2.0 nm) were not detectable using the SMPS for the MSA+TMA+$NH_3$ reaction.

**Figure 6.** (a) Total particle concentrations ($N_{total}$) from MSA+TMA+$NH_3$ reactions for varying $NH_3$ concentrations as a function of reaction time measured using the CPC (dry conditions; each point corresponds to an average from three replicate CPC measurements ± 1 standard deviation made over 2 min each). (b) Enhancement factor for particles measured as a function of $NH_3$ concentration (data for t = 5.9 s). Concentrations of reactants are [MSA] = $6.4 \times 10^{10}$ molecules $cm^{-3}$; [TMA] = $4.8 \times 10^{10}$ molecules $cm^{-3}$; [$NH_3$] = (0-10) $\times 10^{10}$ molecules $cm^{-3}$.

**Figure 7.** (a) Total particle number concentrations ($N_{total}$) from MSA+TMA+$H_2O$ and MSA+TMA+$NH_3$+$H_2O$ reactions as a function of reaction time measured using the CPC (RH ~45-50%). Each data point corresponds to the average $N_{total}$ measured over a 5-min scan (error bars correspond to 1 standard deviation). (b) Comparison of $N_{total}$ values measured at 5.9 s for MSA+$H_2O$+$NH_3$, MSA+$H_2O$+TMA and MSA+$H_2O$+TMA+$NH_3$. Corresponding size distributions for (c) the MSA+TMA+$H_2O$ reaction and (d) the MSA+TMA+$H_2O$+$NH_3$ reactions, respectively. Each size distribution is given in light colors with a log normal fit to guide the eye (each distribution corresponds to an average from five successive scans, except for reaction time 5.9 s where ten scans were averaged instead (standard deviation are not shown for clarity)). Concentrations of reactants for all panels are [MSA] = $7.9 \times 10^{10}$ molecules $cm^{-3}$; [TMA] = 0 or $5.0 \times 10^{10}$ molecules $cm^{-3}$; [$NH_3$] = 0 or $2.2 \times 10^{10}$ molecules $cm^{-3}$.

**Figure 8.** Structures with distances (in angstroms) and partial charges δ (in atomic units) of the most stable structures of complexes composed of MSA, TMA, $NH_3$ and $H_2O$ at the level of B3LYP-D3/aug-cc-pVDZ.

# References

1. M. Kulmala and V. M. Kerminen, On the formation and growth of atmospheric nanoparticles, *Atmos. Res.*, 2008, **90**, 132-150.
2. M. Kulmala, H. Vehkamaki, T. Petaja, M. Dal Maso, A. Lauri, V. M. Kerminen, W. Birmili and P. H. McMurry, Formation and growth rates of ultrafine atmospheric particles: a review of observations, *J. Aerosol Sci.*, 2004, **35**, 143-176.
3. R. Y. Zhang, A. Khalizov, L. Wang, M. Hu and W. Xu, Nucleation and growth of nanoparticles in the atmosphere, *Chem. Rev.*, 2012, **112**, 1957-2011.
4. S. H. Lee, H. Gordon, H. Yu, K. Lehtipalo, R. Haley, Y. X. Li and R. Y. Zhang, New particle formation in the atmosphere: from molecular clusters to global climate, *J. Geophys. Res.*, 2019, **124**, 7098-7146.
5. C. O. Stanier, A. Y. Khlystov and S. N. Pandis, Nucleation events during the Pittsburgh air quality study: Description and relation to key meteorological, gas phase, and aerosol parameters, *Aerosol Sci. Technol.*, 2004, **38**, 253-264.
6. J. N. Smith, M. J. Dunn, T. M. VanReken, K. Iida, M. R. Stolzenburg, P. H. McMurry and L. G. Huey, Chemical composition of atmospheric nanoparticles formed from nucleation in Tecamac, Mexico: Evidence for an important role for organic species in nanoparticle growth, *Geosphys. Res. Lett.*, 2008, **35**, 1-5.
7. H. Yu, A. G. Hallar, Y. You, A. Sedlacek, S. Springston, V. P. Kanawade, Y. N. Lee, J. Wang, C. G. Kuang, R. L. McGraw, I. McCubbin, J. Mikkila and S. H. Lee, Sub-3nm particles observed at the coastal and continental sites in the United States, *J. Geophys. Res.*, 2014, **119**, 860-879.
8. J. M. Makela, S. Yli-Koivisto, V. Hiltunen, W. Seidl, E. Swietlicki, K. Teinila, M. Sillanpaa, I. K. Koponen, J. Paatero, K. Rosman and K. Hameri, Chemical composition of aerosol during particle formation events in boreal forest, *Tellus B*, 2001, **53**, 380-393.
9. P. Pillai, A. Khlystov, J. Walker and V. Aneja, Observation and analysis of particle nucleation at a forest site in Southeastern US, *Atmosphere*, 2013, **4**, 72-93.
10. K. Lehtipalo, M. Sipila, H. Junninen, M. Ehn, T. Berndt, M. K. Kajos, D. R. Worsnop, T. Petaja and M. Kulmala, Observations of nano-CN in the nocturnal boreal forest, *Aerosol Sci. Technol.*, 2011, **45**, 499-509.
11. M. J. Lawler, M. P. Rissanen, M. Ehn, R. L. Mauldin, N. Sarnela, M. Sipila and J. N. Smith, Evidence for diverse biogeochemical drivers of boreal forest new particle formation, *Geosphys. Res. Lett.*, 2018, **45**, 2038-2046.
12. M. J. Lawler, J. Whitehead, C. O'Dowd, C. Monahan, G. McFiggans and J. N. Smith, Composition of 15-85 nm particles in marine air, *Atmos. Chem. Phys.*, 2014, **14**, 11557-11569.
13. R. J. Weber, P. H. McMurry, L. Mauldin, D. J. Tanner, F. L. Eisele, F. J. Brechtel, S. M. Kreidenweis, G. L. Kok, R. D. Schillawski and D. Baumgardner, A study of new particle formation and growth involving biogenic and trace gas species measured during ACE 1, *J. Geophys. Res.*, 1998, **103**, 16385-16396.

14. C. D. O'Dowd, M. Geever and M. K. Hill, New particle formation: Nucleation rates and spatial scales in the clean marine coastal environment, *Geosphys. Res. Lett.*, 1998, **25**, 1661-1664.
15. D. B. Collins, J. Burkart, R. Y. W. Chang, M. Lizotte, A. Boivin-Rioux, M. Blais, E. L. Mungall, M. Boyer, V. E. Irish, G. Masse, D. Kunkel, J. E. Tremblay, T. Papakyriakou, A. K. Bertram, H. Bozem, M. Gosselin, M. Levasseur and J. P. D. Abbatt, Frequent ultrafine particle formation and growth in Canadian Arctic marine and coastal environments, *Atmos. Chem. Phys.*, 2017, **17**, 13119-13138.
16. M. Dall'Osto, D. C. S. Beddows, P. Tunved, R. Krejci, J. Strom, H. C. Hansson, Y. J. Yoon, K. T. Park, S. Becagli, R. Udisti, T. Onasch, C. D. O'Dowd, R. Simo and R. M. Harrison, Arctic sea ice melt leads to atmospheric new particle formation, *Sci. Rep.*, 2017, **7**, 1-10.
17. A. Singh, W. J. Bloss and F. D. Pope, 60 years of UK visibility measurements: Impact of meteorology and atmospheric pollutants on visibility, *Atmos. Chem. Phys.*, 2017, **17**, 2085-2101.
18. W. C. Hinds, *Aerosol Technology: Properties, Behavior, and Measurement of Airborne Particles*, John Wiley & sons Inc., New York, 1999.
19. D. Chang, Y. Song and B. Liu, Visibility trends in six megacities in China 1973-2007, *Atmospheric Research*, 2009, **94**, 161-167.
20. U. Pöschl, Atmospheric aerosols: Composition, transformation, climate and health effects, *Angew. Chem. Int. Ed.*, 2005, **44**, 7520-7540.
21. C. A. Pope and D. W. Dockery, Health effects of fine particulate air pollution: Lines that connect, *J. Air Waste Manage. Assoc.*, 2006, **56**, 709-742.
22. J. L. Mauderly and J. C. Chow, Health effects of organic aerosols, *Inhalation Toxicol.*, 2008, **20**, 257-288.
23. M. R. Heal, P. Kumar and R. M. Harrison, Particles, air quality, policy and health, *Chem. Soc. Rev.*, 2012, **41**, 6606-6630.
24. A. Nel, Air pollution-related illness: Effects of particles, *Science*, 2005, **308**, 804-806.
25. Intergovernmental Panel on Climate Change, *IPPC, Summary for Policymakers in: Climate Change 2013: The Physical Science Basis. Contribution of Working Group I to the Fifth Assessment Report of the Intergovernmental Panel on Climate Change*, Cambridge University Press, Cambridge, United Kingdom and New York, NY, USA, 2013.
26. M. Kanakidou, J. H. Seinfeld, S. N. Pandis, I. Barnes, F. J. Dentener, M. C. Facchini, R. Van Dingenen, B. Ervens, A. Nenes, C. J. Nielsen, E. Swietlicki, J. P. Putaud, Y. Balkanski, S. Fuzzi, J. Horth, G. K. Moortgat, R. Winterhalter, C. E. L. Myhre, K. Tsigaridis, E. Vignati, E. G. Stephanou and J. Wilson, Organic aerosol and global climate modelling: A review, *Atmos. Chem. Phys.*, 2005, **5**, 1053-1123.
27. M. Hallquist, J. C. Wenger, U. Baltensperger, Y. Rudich, D. Simpson, M. Claeys, J. Dommen, N. M. Donahue, C. George, A. H. Goldstein, J. F. Hamilton, H. Herrmann, T. Hoffmann, Y. Iinuma, M. Jang, M. E. Jenkin, J. L. Jimenez, A. Kiendler-Scharr, W. Maenhaut, G. McFiggans, T. F. Mentel, A. Monod, A. S. H. Prevot, J. H. Seinfeld, J. D. Surratt, R. Szmigielski and J. Wildt, The formation, properties and impact of secondary organic aerosol: current and emerging issues, *Atmos. Chem. Phys.*, 2009, **9**, 5155-5236.
28. S. Fuzzi, U. Baltensperger, K. Carslaw, S. Decesari, H. D. van Der Gon, M. C. Facchini, D. Fowler, I. Koren, B. Langford, U. Lohmann, E. Nemitz, S. Pandis, I. Riipinen, Y.

Rudich, M. Schaap, J. G. Slowik, D. V. Spracklen, E. Vignati, M. Wild, M. Williams and S. Gilardoni, Particulate matter, air quality and climate: Lessons learned and future needs, *Atmos. Chem. Phys.*, 2015, **15**, 8217-8299.

29. J. Almeida, S. Schobesberger, A. Kurten, I. K. Ortega, O. Kupiainen-Maatta, A. P. Praplan, A. Adamov, A. Amorim, F. Bianchi, M. Breitenlechner, A. David, J. Dommen, N. M. Donahue, A. Downard, E. Dunne, J. Duplissy, S. Ehrhart, R. C. Flagan, A. Franchin, R. Guida, J. Hakala, A. Hansel, M. Heinritzi, H. Henschel, T. Jokinen, H. Junninen, M. Kajos, J. Kangasluoma, H. Keskinen, A. Kupc, T. Kurten, A. N. Kvashin, A. Laaksonen, K. Lehtipalo, M. Leiminger, J. Leppa, V. Loukonen, V. Makhmutov, S. Mathot, M. J. McGrath, T. Nieminen, T. Olenius, A. Onnela, T. Petaja, F. Riccobono, I. Riipinen, M. Rissanen, L. Rondo, T. Ruuskanen, F. D. Santos, N. Sarnela, S. Schallhart, R. Schnitzhofer, J. H. Seinfeld, M. Simon, M. Sipila, Y. Stozhkov, F. Stratmann, A. Tome, J. Trostl, G. Tsagkogeorgas, P. Vaattovaara, Y. Viisanen, A. Virtanen, A. Vrtala, P. E. Wagner, E. Weingartner, H. Wex, C. Williamson, D. Wimmer, P. L. Ye, T. Yli-Juuti, K. S. Carslaw, M. Kulmala, J. Curtius, U. Baltensperger, D. R. Worsnop, H. Vehkamaki and J. Kirkby, Molecular understanding of sulphuric acid-amine particle nucleation in the atmosphere, *Nature*, 2013, **502**, 359-363.
30. T. Kurten, V. Loukonen, H. Vehkamaki and M. Kulmala, Amines are likely to enhance neutral and ion-induced sulfuric acid-water nucleation in the atmosphere more effectively than ammonia, *Atmos. Chem. Phys.*, 2008, **8**, 4095-4103.
31. H. Yu, R. McGraw and S. H. Lee, Effects of amines on formation of sub-3 nm particles and their subsequent growth, *Geosphys. Res. Lett.*, 2012, **39**, 1-5.
32. W. A. Glasoe, K. Volz, B. Panta, N. Freshour, R. Bachman, D. R. Hanson, P. H. McMurry and C. Jen, Sulfuric acid nucleation: An experimental study of the effect of seven bases, *J. Geophys. Res.*, 2015, **120**, 1933-1950.
33. J. H. Zollner, W. A. Glasoe, B. Panta, K. K. Carlson, P. H. McMurry and D. R. Hanson, Sulfuric acid nucleation: power dependencies, variation with relative humidity, and effect of bases, *Atmos. Chem. Phys.*, 2012, **12**, 4399-4411.
34. J. Kirkby, J. Curtius, J. Almeida, E. Dunne, J. Duplissy, S. Ehrhart, A. Franchin, S. Gagne, L. Ickes, A. Kurten, A. Kupc, A. Metzger, F. Riccobono, L. Rondo, S. Schobesberger, G. Tsagkogeorgas, D. Wimmer, A. Amorim, F. Bianchi, M. Breitenlechner, A. David, J. Dommen, A. Downard, M. Ehn, R. C. Flagan, S. Haider, A. Hansel, D. Hauser, W. Jud, H. Junninen, F. Kreissl, A. Kvashin, A. Laaksonen, K. Lehtipalo, J. Lima, E. R. Lovejoy, V. Makhmutov, S. Mathot, J. Mikkila, P. Minginette, S. Mogo, T. Nieminen, A. Onnela, P. Pereira, T. Petaja, R. Schnitzhofer, J. H. Seinfeld, M. Sipila, Y. Stozhkov, F. Stratmann, A. Tome, J. Vanhanen, Y. Viisanen, A. Vrtala, P. E. Wagner, H. Walther, E. Weingartner, H. Wex, P. M. Winkler, K. S. Carslaw, D. R. Worsnop, U. Baltensperger and M. Kulmala, Role of sulphuric acid, ammonia and galactic cosmic rays in atmospheric aerosol nucleation, *Nature*, 2011, **476**, 429-433.
35. L. Yao, O. Garmash, F. Bianchi, J. Zheng, C. Yan, J. Kontkanen, H. Junninen, S. B. Mazon, M. Ehn, P. Paasonen, M. Sipila, M. Y. Wang, X. K. Wang, S. Xiao, H. F. Chen, Y. Q. Lu, B. W. Zhang, D. F. Wang, Q. Y. Fu, F. H. Geng, L. Li, H. L. Wang, L. P. Qiao, X. Yang, J. M. Chen, V. M. Kerminen, T. Petaja, D. R. Worsnop, M. Kulmala and L. Wang, Atmospheric new particle formation from sulfuric acid and amines in a Chinese megacity, *Science*, 2018, **361**, 278-281.

36. C. N. Jen, R. Bachman, J. Zhao, P. H. McMurry and D. R. Hanson, Diamine-sulfuric acid reactions are a potent source of new particle formation, *Geosphys. Res. Lett.*, 2016, **43**, 867-873.
37. C. N. Jen, P. H. McMurry and D. R. Hanson, Stabilization of sulfuric acid dimers by ammonia, methylamine, dimethylamine, and trimethylamine, *J. Geophys. Res.*, 2014, **119**, 7502-7514.
38. J. Zhao, J. N. Smith, F. L. Eisele, M. Chen, C. Kuang and P. H. McMurry, Observation of neutral sulfuric acid-amine containing clusters in laboratory and ambient measurements, *Atmos. Chem. Phys.*, 2011, **11**, 10823-10836.
39. J. Elm, M. Passananti, T. Kurten and H. Vehkamaki, Diamines can initiate new particle formation in the atmosphere, *J. Phys. Chem. A*, 2017, **121**, 6155-6164.
40. H. B. Xie, J. Elm, R. Halonen, N. Myllys, T. Kurten, M. Kulmala and H. Vehkamaki, Atmospheric fate of monoethanolamine: enhancing new particle formation of sulfuric acid as an important removal process, *Environ. Sci. Technol.*, 2017, **51**, 8422-8431.
41. T. Berndt, F. Stratmann, M. Sipila, J. Vanhanen, T. Petaja, J. Mikkila, A. Gruner, G. Spindler, R. L. Mauldin, J. Curtius, M. Kulmala and J. Heintzenberg, Laboratory study on new particle formation from the reaction OH + $SO_2$: influence of experimental conditions, $H_2O$ vapour, $NH_3$ and the amine tert-butylamine on the overall process, *Atmos. Chem. Phys.*, 2010, **10**, 7101-7116.
42. T. Berndt, M. Sipila, F. Stratmann, T. Petaja, J. Vanhanen, J. Mikkila, J. Patokoski, R. Taipale, R. L. Mauldin and M. Kulmala, Enhancement of atmospheric $H_2SO_4/H_2O$ nucleation: organic oxidation products versus amines, *Atmos. Chem. Phys.*, 2014, **14**, 751-764.
43. M. E. Erupe, A. A. Viggiano and S. H. Lee, The effect of trimethylamine on atmospheric nucleation involving $H_2SO_4$, *Atmos. Chem. Phys.*, 2011, **11**, 4767-4775.
44. T. Olenius, R. Halonen, T. Kurten, H. Henschel, O. Kupiainen-Maata, I. K. Ortega, C. N. Jen, H. Vehkamaki and I. Riipinen, New particle formation from sulfuric acid and amines: Comparison of monomethylamine, dimethylamine, and trimethylamine, *J. Geophys. Res.*, 2017, **122**, 7103-7118.
45. A. Kurten, F. Bianchi, J. Almeida, O. Kupiainen-Maatta, E. M. Dunne, J. Duplissy, C. Williamson, P. Barmet, M. Breitenlechner, J. Dommen, N. M. Donahue, R. C. Flagan, A. Franchin, H. Gordon, J. Hakala, A. Hansel, M. Heinritzi, L. Ickes, T. Jokinen, J. Kangasluoma, J. Kim, J. Kirkby, A. Kupc, K. Lehtipalo, M. Leiminger, V. Makhmutov, A. Onnela, I. K. Ortega, T. Petaja, A. P. Praplan, F. Riccobono, M. P. Rissanen, L. Rondo, R. Schnitzhofer, S. Schobesberger, J. N. Smith, G. Steiner, Y. Stozhkov, A. Tome, J. Trostl, G. Tsagkogeorgas, P. E. Wagner, D. Wimmer, P. L. Ye, U. Baltensperger, K. Carslaw, M. Kulmala and J. Curtius, Experimental particle formation rates spanning tropospheric sulfuric acid and ammonia abundances, ion production rates, and temperatures, *J. Geophys. Res.*, 2016, **121**, 12377-12400.
46. S. M. Ball, D. R. Hanson, F. L. Eisele and P. H. McMurry, Laboratory studies of particle nucleation: Initial results for $H_2SO_4$, $H_2O$, and $NH_3$ vapors, *J. Geophys. Res.*, 1999, **104**, 23709-23718.
47. D. R. Benson, M. E. Erupe and S. H. Lee, Laboratory-measured $H_2SO_4$-$H_2O$-$NH_3$ ternary homogeneous nucleation rates: initial observations, *Geosphys. Res. Lett.*, 2009, **36**, 1-6.
48. K. Lehtipalo, L. Rondo, J. Kontkanen, S. Schobesberger, T. Jokinen, N. Sarnela, A. Kurten, S. Ehrhart, A. Franchin, T. Nieminen, F. Riccobono, M. Sipila, T. Yli-Juuti, J.

Duplissy, A. Adamov, L. Ahlm, J. Almeida, A. Amorim, F. Bianchi, M. Breitenlechner, J. Dommen, A. J. Downard, E. M. Dunne, R. C. Flagan, R. Guida, J. Hakala, A. Hansel, W. Jud, J. Kangasluoma, V. M. Kerminen, H. Keskinen, J. Kim, J. Kirkby, A. Kupc, O. Kupiainen-Maatta, A. Laaksonen, M. J. Lawler, M. Leiminger, S. Mathot, T. Olenius, I. K. Ortega, A. Onnela, T. Petaja, A. Praplan, M. P. Rissanen, T. Ruuskanen, F. D. Santos, S. Schallhart, R. Schnitzhofer, M. Simon, J. N. Smith, J. Trostl, G. Tsagkogeorgas, A. Tome, P. Vaattovaara, H. Vehkamaki, A. E. Vrtala, P. E. Wagner, C. Williamson, D. Wimmer, P. M. Winkler, A. Virtanen, N. M. Donahue, K. S. Carslaw, U. Baltensperger, I. Riipinen, J. Curtius, D. R. Worsnop and M. Kulmala, The effect of acid-base clustering and ions on the growth of atmospheric nano-particles, *Nat. Commun.*, 2016, **7**, 1-9.

49. M. Chen, M. Titcombe, J. K. Jiang, C. Jen, C. A. Kuang, M. L. Fischer, F. L. Eisele, J. I. Siepmann, D. R. Hanson, J. Zhao and P. H. McMurry, Acid-base chemical reaction model for nucleation rates in the polluted atmospheric boundary layer, *Proc. Natl. Acad. Sci. USA*, 2012, **109**, 18713-18718.

50. J. N. Smith, K. F. Moore, F. L. Eisele, D. Voisin, A. K. Ghimire, H. Sakurai and P. H. McMurry, Chemical composition of atmospheric nanoparticles during nucleation events in Atlanta, *J. Geophys. Res.*, 2005, **110**, 1-13.

51. A. Kurten, T. Jokinen, M. Simon, M. Sipila, N. Sarnela, H. Junninen, A. Adamov, J. Almeida, A. Amorim, F. Bianchi, M. Breitenlechner, J. Dommen, N. M. Donahue, J. Duplissy, S. Ehrhart, R. C. Flagan, A. Franchin, J. Hakala, A. Hansel, M. Heinritzi, M. Hutterli, J. Kangasluoma, J. Kirkby, A. Laaksonen, K. Lehtipalo, M. Leiminger, V. Makhmutov, S. Mathot, A. Onnela, T. Petaja, A. P. Praplan, F. Riccobono, M. P. Rissanen, L. Rondo, S. Schobesberger, J. H. Seinfeld, G. Steiner, A. Tome, J. Trostl, P. M. Winkler, C. Williamson, D. Wimmer, P. L. Ye, U. Baltensperger, K. S. Carslaw, M. Kulmala, D. R. Worsnop and J. Curtius, Neutral molecular cluster formation of sulfuric acid-dimethylamine observed in real time under atmospheric conditions, *Proc. Natl. Acad. Sci. USA*, 2014, **111**, 15019-15024.

52. F. Bianchi, A. P. Praplan, N. Sarnela, J. Dommen, A. Kurten, I. K. Ortega, S. Schobesberger, H. Junninen, M. Simon, J. Trostl, T. Jokinen, M. Sipila, A. Adamov, A. Amorim, J. Almeida, M. Breitenlechner, J. Duplissy, S. Ehrhart, R. C. Flagan, A. Franchin, J. Hakala, A. Hansel, M. Heinritzi, J. Kangasluoma, H. Keskinen, J. Kim, J. Kirkby, A. Laaksonen, M. J. Lawler, K. Lehtipalo, M. Leiminger, V. Makhmutov, S. Mathot, A. Onnela, T. Petaja, F. Riccobono, M. P. Rissanen, L. Rondo, A. Tome, A. Virtanen, Y. Viisanen, C. Williamson, D. Wimmer, P. M. Winkler, P. L. Ye, J. Curtius, M. Kulmala, D. R. Worsnop, N. M. Donahue and U. Baltensperger, Insight into acid-base nucleation experiments by comparison of the chemical composition of positive, negative, and neutral clusters, *Environ. Sci. Technol.*, 2014, **48**, 13675-13684.

53. S. Schobesberger, A. Franchin, F. Bianchi, L. Rondo, J. Duplissy, A. Kurten, I. K. Ortega, A. Metzger, R. Schnitzhofer, J. Almeida, A. Amorim, J. Dommen, E. M. Dunne, M. Ehn, S. Gagne, L. Ickes, H. Junninen, A. Hansel, V. M. Kerminen, J. Kirkby, A. Kupc, A. Laaksonen, K. Lehtipalo, S. Mathot, A. Onnela, T. Petaja, F. Riccobono, F. D. Santos, M. Sipila, A. Tome, G. Tsagkogeorgas, Y. Viisanen, P. E. Wagner, D. Wimmer, J. Curtius, N. M. Donahue, U. Baltensperger, M. Kulmala and D. R. Worsnop, On the composition of ammonia-sulfuric-acid ion clusters during aerosol particle formation, *Atmos. Chem. Phys.*, 2015, **15**, 55-78.

54. I. K. Ortega, O. Kupiainen, T. Kurten, T. Olenius, O. Wilkman, M. J. McGrath, V. Loukonen and H. Vehkamaki, From quantum chemical formation free energies to evaporation rates, *Atmos. Chem. Phys.*, 2012, **12**, 225-235.
55. V. Loukonen, T. Kurten, I. K. Ortega, H. Vehkamaki, A. A. H. Padua, K. Sellegri and M. Kulmala, Enhancing effect of dimethylamine in sulfuric acid nucleation in the presence of water - a computational study, *Atmos. Chem. Phys.*, 2010, **10**, 4961-4974.
56. J. W. DePalma, D. J. Doren and M. V. Johnston, Formation and growth of molecular clusters containing sulfuric acid, water, ammonia, and dimethylamine, *J. Phys. Chem. A*, 2014, **118**, 5464-5473.
57. L. J. Larson, A. Largent and F. M. Tao, Structure of the sulfuric acid-ammonia system and the effect of water molecules in the gas phase, *J. Phys. Chem. A*, 1999, **103**, 6786-6792.
58. H. Henschel, T. Kurten and H. Vehkamaki, Computational study on the effect of hydration on new particle formation in the sulfuric acid/ammonia and sulfuric acid/dimethylamine systems, *J. Phys. Chem. A*, 2016, **120**, 1886-1896.
59. J. N. Smith, K. C. Barsanti, H. R. Friedli, M. Ehn, M. Kulmala, D. R. Collins, J. H. Scheckman, B. J. Williams and P. H. McMurry, Observations of aminium salts in atmospheric nanoparticles and possible climatic implications, *Proc. Natl. Acad. Sci. USA*, 2010, **107**, 6634-6639.
60. B. R. Bzdek, M. J. Lawler, A. J. Horan, M. R. Pennington, J. W. DePalma, J. Zhao, J. N. Smith and M. V. Johnston, Molecular constraints on particle growth during new particle formation, *Geosphys. Res. Lett.*, 2014, **41**, 6045-6054.
61. J. M. Creamean, A. P. Ault, J. E. Ten Hoeve, M. Z. Jacobson, G. C. Roberts and K. A. Prather, Measurements of aerosol chemistry during new particle formation events at a remote rural mountain site, *Environ. Sci. Technol.*, 2011, **45**, 8208-8216.
62. A. Kurten, A. Bergen, M. Heinritzi, M. Leiminger, V. Lorenz, F. Piel, M. Simon, R. Sitals, A. C. Wagner and J. Curtius, Observation of new particle formation and measurement of sulfuric acid, ammonia, amines and highly oxidized organic molecules at a rural site in central Germany, *Atmos. Chem. Phys.*, 2016, **16**, 12793-12813.
63. Q. Zhang, C. O. Stanier, M. R. Canagaratna, J. T. Jayne, D. R. Worsnop, S. N. Pandis and J. L. Jimenez, Insights into the chemistry of new particle formation and growth events in Pittsburgh based on aerosol mass spectrometry, *Environ. Sci. Technol.*, 2004, **38**, 4797-4809.
64. S. Schobesberger, H. Junninen, F. Bianchi, G. Lonn, M. Ehn, K. Lehtipalo, J. Dommen, S. Ehrhart, I. K. Ortega, A. Franchin, T. Nieminen, F. Riccobono, M. Hutterli, J. Duplissy, J. Almeida, A. Amorim, M. Breitenlechner, A. J. Downard, E. M. Dunne, R. C. Flagan, M. Kajos, H. Keskinen, J. Kirkby, A. Kupc, A. Kurten, T. Kurten, A. Laaksonen, S. Mathot, A. Onnela, A. P. Praplan, L. Rondo, F. D. Santos, S. Schallhart, R. Schnitzhofer, M. Sipila, A. Tome, G. Tsagkogeorgas, H. Vehkamaki, D. Wimmer, U. Baltensperger, K. S. Carslaw, J. Curtius, A. Hansel, T. Petaja, M. Kulmala, N. M. Donahue and D. R. Worsnop, Molecular understanding of atmospheric particle formation from sulfuric acid and large oxidized organic molecules, *Proc. Natl. Acad. Sci. USA*, 2013, **110**, 17223-17228.
65. M. R. Pennington, B. R. Bzdek, J. W. DePalma, J. N. Smith, A. M. Kortelainen, L. Hildebrandt Ruiz, T. Petaja, M. Kulmala, D. R. Worsnop and M. V. Johnston,

Identification and quantification of particle growth channels during new particle formation, *Atmos. Chem. Phys.*, 2013, **13**, 10215-10225.

66. S. Chee, N. Myllys, K. C. Barsanti, B. M. Wong and J. N. Smith, An experimental and modeling study of nanoparticle formation and growth from dimethylamine and nitric acid, *J. Phys. Chem. A*, 2019, **123**, 5640-5648.
67. S. M. Murphy, A. Sorooshian, J. H. Kroll, N. L. Ng, P. Chhabra, C. Tong, J. D. Surratt, E. Knipping, R. C. Flagan and J. H. Seinfeld, Secondary aerosol formation from atmospheric reactions of aliphatic amines, *Atmos. Chem. Phys.*, 2007, **7**, 2313-2337.
68. I. Napari, M. Kulmala and H. Vehkamaki, Ternary nucleation of inorganic acids, ammonia, and water, *J. Chem. Phys.*, 2002, **117**, 8418-8425.
69. F. M. Tao, Gas phase proton transfer reaction of nitric acid ammonia and the role of water, *J. Chem. Phys.*, 1998, **108**, 193-202.
70. F. M. Tao, Direct formation of solid ammonium chloride particles from HCl and $NH_3$ vapors, *J. Chem. Phys.*, 1999, **110**, 11121-11124.
71. M. Luria and B. Cohen, Kinetics of gas to particle conversion in the $NH_3$-HCl system, *Atmos. Environ.*, 1980, **14**, 665-670.
72. J. Chen, S. Jiang, Y. R. Liu, T. Huang, C. Y. Wang, S. K. Miao, Z. Q. Wang, Y. Zhang and W. Huang, Interaction of oxalic acid with dimethylamine and its atmospheric implications, *RSC Adv.*, 2017, **7**, 6374-6388.
73. K. D. Arquero, R. B. Gerber and B. J. Finlayson-Pitts, The role of oxalic acid in new particle formation from methanesulfonic acid, methylamine, and water, *Environ. Sci. Technol.*, 2017, **51**, 2124-2130.
74. K. D. Arquero, J. Xu, R. B. Gerber and B. J. Finlayson-Pitts, Particle formation and growth from oxalic acid, methanesulfonic acid, trimethylamine and water: a combined experimental and theoretical study, *Phys. Chem. Chem. Phys.*, 2017, **19**, 28286-28301.
75. J. Zhao, A. Khalizov, R. Y. Zhang and R. McGraw, Hydrogen-bonding interaction in molecular complexes and clusters of aerosol nucleation precursors, *J. Phys. Chem. A*, 2009, **113**, 680-689.
76. W. Xu and R. Y. Zhang, A theoretical study of hydrated molecular clusters of amines and dicarboxylic acids, *J. Chem. Phys.*, 2013, **139**, 1-11.
77. K. H. Weber, Q. Liu and F. M. Tao, Theoretical study on stable small clusters of oxalic acid with ammonia and water, *J. Phys. Chem. A*, 2014, **118**, 1451-1468.
78. X. Q. Peng, T. Huang, S. K. Miao, J. Chen, H. Wen, Y. J. Feng, Y. Hong, C. Y. Wang and W. Huang, Hydration of oxalic acid-ammonia complex: atmospheric implication and Rayleigh-scattering properties, *RSC Adv.*, 2016, **6**, 46582-46593.
79. X. Q. Peng, Y. R. Liu, T. Huang, S. Jiang and W. Huang, Interaction of gas phase oxalic acid with ammonia and its atmospheric implications, *Phys. Chem. Chem. Phys.*, 2015, **17**, 9552-9563.
80. S. Patai and Z. Rappoport, *The Chemistry of suphonic acids, esters and derivatives*, John Wiley & Sons Ltd, New York, 1991.
81. I. Barnes, J. Hjorth and N. Mihalopoulos, Dimethyl sulfide and dimethyl sulfoxide and their oxidation in the atmosphere, *Chem. Rev.*, 2006, **106**, 940-975.
82. M. L. Dawson, M. E. Varner, V. Perraud, M. J. Ezell, R. B. Gerber and B. J. Finlayson-Pitts, Simplified mechanism for new particle formation from methanesulfonic acid, amines, and water via experiments and ab initio calculations, *Proc. Natl. Acad. Sci. USA*, 2012, **109**, 18719-18724.

83. H. H. Chen, M. J. Ezell, K. D. Arquero, M. E. Varner, M. L. Dawson, R. B. Gerber and B. J. Finlayson-Pitts, New particle formation and growth from methanesulfonic acid, trimethylamine and water, *Phys. Chem. Chem. Phys.*, 2015, **17**, 13699-13709.
84. H. H. Chen and B. J. Finlayson-Pitts, New particle formation from methanesulfonic acid and amines/ammonia as a function of temperature, *Environ. Sci. Technol.*, 2017, **51**, 243-252.
85. H. H. Chen, M. E. Varner, R. B. Gerber and B. J. Finlayson-Pitts, Reactions of methanesulfonic acid with amines and ammonia as a source of new particles in air, *J. Phys. Chem. B*, 2016, **120**, 1526-1536.
86. Z. Klimont, S. J. Smith and J. Cofala, The last decade of global anthropogenic sulfur dioxide: 2000-2011 emissions, *Environ Res Lett*, 2013, **8**, 1-6.
87. M. Amann, Z. Klimont and F. Wagner, Regional and global emissions of air pollutants: Recent trends and future scenarios, *Ann. Rev. Environ. Resour.*, 2013, **38**, 31-55.
88. V. Perraud, J. R. Horne, A. S. Martinez, J. Kalinowski, S. Meinardi, M. L. Dawson, L. M. Wingen, D. Dabdub, D. R. Blake, R. B. Gerber and B. J. Finlayson-Pitts, The future of airborne sulfur-containing particles in the absence of fossil fuel sulfur dioxide emissions, *Proc. Natl. Acad. Sci. USA*, 2015, **112**, 13514-13519.
89. J. G. Murphy, P. K. Gregoire, A. G. Tevlin, G. R. Wentworth, R. A. Ellis, M. Z. Markovic and T. C. VandenBoer, Observational constraints on particle acidity using measurements and modelling of particles and gases, *Faraday Discuss.*, 2017, **200**, 379-395.
90. D. I. Stern, Global sulfur emissions from 1850 to 2000, *Chemosphere*, 2005, **58**, 163-175.
91. U.S. EPA., https://www.epa.gov/air-trends/sulfur-dioxide-trends, (accessed Sept. 16, 2019).
92. H. Berresheim, M. Adam, C. Monahan, C. O'Dowd, J. M. C. Plane, B. Bohn and F. Rohrer, Missing $SO_2$ oxidant in the coastal atmosphere? - Observations from high-resolution measurements of OH and atmospheric sulfur compounds, *Atmos. Chem. Phys.*, 2014, **14**, 12209-12223.
93. H. Berresheim, F. L. Eisele, D. J. Tanner, L. M. Mcinnes, D. C. Ramseybell and D. S. Covert, Atmospheric sulfur chemistry and cloud condensation nuclei (CCN) concentrations over the Northeastern Pacific Coast, *J. Geophys. Res.*, 1993, **98**, 12701-12711.
94. H. Berresheim, T. Elste, H. G. Tremmel, A. G. Allen, H. C. Hansson, K. Rosman, M. Dal Maso, J. M. Makela, M. Kulmala and C. D. O'Dowd, Gas-aerosol relationships of $H_2SO_4$, MSA, and OH: Observations in the coastal marine boundary layer at Mace Head, Ireland, *J. Geophys. Res.*, 2002, **107**, 1-12.
95. F. L. Eisele and D. J. Tanner, Measurement of the gas-phase concentration of $H_2SO_4$ and methane sulfonic-acid and estimates of $H_2SO_4$ production and loss in the atmosphere, *J. Geophys. Res.*, 1993, **98**, 9001-9010.
96. R. L. Mauldin, C. A. Cantrell, M. A. Zondlo, E. Kosciuch, B. A. Ridley, R. Weber and F. E. Eisele, Measurements of OH, $H_2SO_4$, and MSA during Tropospheric Ozone Production about the Spring Equinox (TOPSE), *J. Geophys. Res.*, 2003, **108**, 1-18.
97. R. L. Mauldin, D. J. Tanner, J. A. Heath, B. J. Huebert and F. L. Eisele, Observations of $H_2SO_4$ and MSA during PEM-Tropics-A, *J. Geophys. Res.*, 1999, **104**, 5801-5816.
98. H. Bardouki, H. Berresheim, M. Vrekoussis, J. Sciare, G. Kouvarakis, K. Oikonomou, J. Schneider and N. Mihalopoulos, Gaseous (DMS, MSA, $SO_2$, $H_2SO_4$ and DMSO) and

particulate (sulfate and methanesulfonate) sulfur species over the northeastern coast of Crete, *Atmos. Chem. Phys.*, 2003, **3**, 1871-1886.

99. A. Jefferson, D. J. Tanner, F. L. Eisele, D. D. Davis, G. Chen, J. Crawford, J. W. Huey, A. L. Torres and H. Berresheim, OH photochemistry and methane sulfonic acid formation in the coastal Antarctic boundary layer, *J. Geophys. Res.*, 1998, **103**, 1647-1656.
100. M. C. Facchini, S. Decesari, M. Rinaldi, C. Carbone, E. Finessi, M. Mircea, S. Fuzzi, F. Moretti, E. Tagliavini, D. Ceburnis and C. D. O'Dowd, Important source of marine secondary organic aerosol from biogenic amines, *Environ. Sci. Technol.*, 2008, **42**, 9116-9121.
101. V. M. Kerminen, M. Aurela, R. E. Hillamo and A. Virkkula, Formation of particulate MSA: Deductions from size distribution measurements in the Finnish Arctic, *Tellus B*, 1997, **49**, 159-171.
102. L. N. Kolaitis, F. J. Bruynseels, R. E. Vangrieken and M. O. Andreae, Determination of methanesulfonic-acid and non-sea-salt sulfate in single marine aerosol-particles, *Environ. Sci. Technol.*, 1989, **23**, 236-240.
103. B. R. Bzdek, D. P. Ridge and M. V. Johnston, Reactivity of methanesulfonic acid salt clusters relevant to marine air, *J. Geophys. Res.*, 2011, **116**, Artn D03301, doi: 03310.01029/02010jd015217.
104. B. R. Bzdek, D. P. Ridge and M. V. Johnston, Amine reactivity with charged sulfuric acid clusters, *Atmos. Chem. Phys.*, 2011, **11**, 8735-8743.
105. L. P. Chan and C. K. Chan, Displacement of ammonium from aerosol particles by uptake of triethylamine, *Aerosol Sci. Technol.*, 2012, **46**, 236-247.
106. C. Qiu, L. Wang, V. Lal, A. F. Khalizov and R. Y. Zhang, Heterogeneous reactions of alkylamines with ammonium sulfate and ammonium bisulfate, *Environ. Sci. Technol.*, 2011, **45**, 4748-4755.
107. N. Bork, J. Elm, T. Olenius and H. Vehkamaki, Methane sulfonic acid-enhanced formation of molecular clusters of sulfuric acid and dimethyl amine, *Atmos. Chem. Phys.*, 2014, **14**, 12023-12030.
108. H. J. Zhang, O. Kupiainen-Maatta, X. H. Zhang, V. Molinero, Y. H. Zhang and Z. S. Li, The enhancement mechanism of glycolic acid on the formation of atmospheric sulfuric acid-ammonia molecular clusters, *J. Chem. Phys.*, 2017, **146**, 1-11.
109. Y. Lin, Y. M. Ji, Y. X. Li, J. Secrest, W. Xu, F. Xu, Y. Wang, T. C. An and R. Y. Zhang, Interaction between succinic acid and sulfuric acid-base clusters, *Atmos. Chem. Phys.*, 2019, **19**, 8003-8019.
110. W. Xu and R. Y. Zhang, Theoretical investigation of interaction of dicarboxylic acids with common aerosol nucleation precursors, *J. Phys. Chem. A*, 2012, **116**, 4539-4550.
111. M. J. Lawler, P. M. Winkler, J. Kim, L. Ahlm, J. Trostl, A. P. Praplan, S. Schobesberger, A. Kurten, J. Kirkby, F. Bianchi, J. Duplissy, A. Hansel, T. Jokinen, H. Keskinen, K. Lehtipalo, M. Leiminger, T. Petaja, M. Rissanen, L. Rondo, M. Simon, M. Sipila, C. Williamson, D. Wimmer, I. Riipinen, A. Virtanen and J. N. Smith, Unexpectedly acidic nanoparticles formed in dimethylamine-ammonia-sulfuric-acid nucleation experiments at CLOUD, *Atmos. Chem. Phys.*, 2016, **16**, 13601-13618.
112. N. Myllys, S. Chee, T. Olenius, M. Lawler and J. N. Smith, Molecular-level understanding of synergistic effects in sulfuric acid-amine-ammonia mixed clusters, *J. Phys. Chem. A*, 2019, **123**, 2420-2425.

113. B. Temelso, E. F. Morrison, D. L. Speer, B. C. Cao, N. Appiah-Padi, G. Kim and G. C. Shields, Effect of mixing ammonia and alkylamines on sulfate aerosol formation, *J. Phys. Chem. A*, 2018, **122**, 1612-1622.
114. C. Y. Wang, S. Jiang, Y. R. Liu, H. Wen, Z. Q. Wang, Y. J. Han, T. Huang and W. Huang, Synergistic effect of ammonia and methylamine on nucleation in the Earth's atmosphere. A theoretical study, *J. Phys. Chem. A*, 2018, **122**, 3470-3479.
115. X. L. Ge, A. S. Wexler and S. L. Clegg, Atmospheric amines - Part I. A review, *Atmos. Environ.*, 2011, **45**, 524-546.
116. M. L. Dawson, V. Perraud, A. Gomez, K. D. Arquero, M. J. Ezell and B. J. Finlayson-Pitts, Measurement of gas-phase ammonia and amines in air by collection onto an ion exchange resin and analysis by ion chromatography, *Atmos. Meas. Tech.*, 2014, **7**, 2733-2744.
117. G. W. Schade and P. J. Crutzen, Emission of aliphatic-amines from animal husbandry and their reactions - Potential Source of $N_2O$ and HCN, *J. Atmos. Chem.*, 1995, **22**, 319-346.
118. I. H. Chang, C. G. Lee and D. S. Lee, Development of an automated method for simultaneous determination of low molecular weight aliphatic amines and ammonia in ambient air by diffusion scrubber coupled to ion chromatography, *Anal. Chem.*, 2003, **75**, 6141-6146.
119. J. Xu, B. J. Finlayson-Pitts and R. B. Gerber, Proton transfer in mixed clusters of methanesulfonic acid, methylamine, and oxalic acid: implications for atmospheric particle formation, *J. Phys. Chem. A*, 2017, **121**, 2377-2385.
120. S. J. Li, L. L. Zhang, W. Qin and F. M. Tao, Intermolecular structure and properties of the methanesulfonic acid-ammonia system in small water clusters, *Chem. Phys. Lett.*, 2007, **447**, 33-38.
121. M. Kumar and J. S. Francisco, Ion pair particles at the air-water interface, *Proc. Natl. Acad. Sci. USA*, 2017, **114**, 12401-12406.
122. S. W. Gibb, R. F. C. Mantoura and P. S. Liss, Ocean-atmosphere exchange and atmospheric speciation of ammonia and methylamines in the region of the NW Arabian Sea, *Global Biogeochem. Cycles*, 1999, **13**, 161-177.
123. A. Vanneste, R. A. Duce and C. Lee, Methylamines in the marine atmosphere, *Geosphys. Res. Lett.*, 1987, **14**, 711-714.
124. D. R. Hanson, P. H. McMurry, J. Jiang, D. Tanner and L. G. Huey, Ambient pressure proton transfer mass spectrometry: detection of amines and ammonia, *Environ. Sci. Technol.*, 2011, **45**, 8881-8888.
125. H. Yu and S. H. Lee, Chemical ionisation mass spectrometry for the measurement of atmospheric amines, *Environ. Chem.*, 2012, **9**, 190-201.
126. H. Hellen, A. J. Kieloaho and H. Hakola, Gas-phase alkyl amines in urban air; comparison with a boreal forest site and importance for local atmospheric chemistry, *Atmos. Environ.*, 2014, **94**, 192-197.
127. L. Yao, M. Y. Wang, X. K. Wang, Y. J. Liu, H. F. Chen, J. Zheng, W. Nie, A. J. Ding, F. H. Geng, D. F. Wang, J. M. Chen, D. R. Worsnop and L. Wang, Detection of atmospheric gaseous amines and amides by a high-resolution time-of-flight chemical ionization mass spectrometer with protonated ethanol reagent ions, *Atmos. Chem. Phys.*, 2016, **16**, 14527-14543.

128. T. C. VandenBoer, A. Petroff, M. Z. Markovic and J. G. Murphy, Size distribution of alkyl amines in continental particulate matter and their online detection in the gas and particle phase, *Atmos. Chem. Phys.*, 2011, **11**, 4319-4332.
129. T. C. VandenBoer, M. Z. Markovic, A. Petroff, M. F. Czar, N. Borduas and J. G. Murphy, Ion chromatographic separation and quantitation of alkyl methylamines and ethylamines in atmospheric gas and particulate matter using preconcentration and suppressed conductivity detection, *J. Chromatogr. A*, 2012, **1252**, 74-83.
130. N. A. Freshour, K. K. Carlson, Y. A. Melka, S. Hinz, B. Panta and D. R. Hanson, Amine permeation sources characterized with acid neutralization and sensitivities of an amine mass spectrometer, *Atmos. Meas. Tech.*, 2014, **7**, 3611-3621.
131. J. Sintermann, S. Schallhart, M. Kajos, M. Jocher, A. Bracher, A. Munger, D. Johnson, A. Neftel and T. Ruuskanen, Trimethylamine emissions in animal husbandry, *Biogeosciences*, 2014, **11**, 5073-5085.
132. Y. You, V. P. Kanawade, J. A. de Gouw, A. B. Guenther, S. Madronich, M. R. Sierra-Hernandez, M. Lawler, J. N. Smith, S. Takahama, G. Ruggeri, A. Koss, K. Olson, K. Baumann, R. J. Weber, A. Nenes, H. Guo, E. S. Edgerton, L. Porcelli, W. H. Brune, A. H. Goldstein and S. H. Lee, Atmospheric amines and ammonia measured with a chemical ionization mass spectrometer (CIMS), *Atmos. Chem. Phys.*, 2014, **14**, 12181-12194.
133. J. M. Lobert, D. H. Scharffe, W. M. Hao and P. J. Crutzen, Importance of biomass burning in the atmospheric budgets of nitrogen-containing gases, *Nature*, 1990, **346**, 552-554.
134. K. Sellegri, M. Hanke, B. Umann, F. Arnold and M. Kulmala, Measurements of organic gases during aerosol formation events in the boreal forest atmosphere during QUEST, *Atmos. Chem. Phys.*, 2005, **5**, 373-384.
135. A. J. Kieloaho, H. Hellen, H. Hakola, H. E. Manninen, T. Nieminen, M. Kulmala and M. Pihlatie, Gas-phase alkylamines in a boreal Scots pine forest air, *Atmos. Environ.*, 2013, **80**, 369-377.
136. M. Hemmila, H. Hellen, A. Virkkula, U. Makkonen, A. P. Praplan, J. Kontkanen, L. Ahonen, M. Kulmala and H. Hakola, Amines in boreal forest air at SMEAR II station in Finland, *Atmos. Chem. Phys.*, 2018, **18**, 6367-6380.
137. A. Sorooshian, L. T. Padro, A. Nenes, G. Feingold, A. McComiskey, S. P. Hersey, H. Gates, H. H. Jonsson, S. D. Miller, G. L. Stephens, R. C. Flagan and J. H. Seinfeld, On the link between ocean biota emissions, aerosol, and maritime clouds: Airborne, ground, and satellite measurements off the coast of California, *Global Biogeochem. Cycles*, 2009, **23**, 1-15.
138. C. J. Gaston, K. A. Pratt, X. Y. Qin and K. A. Prather, Real-time detection and mixing state of methanesulfonate in single particles at an inland urban location during a phytoplankton bloom, *Environ. Sci. Technol.*, 2010, **44**, 1566-1572.
139. F. Kollner, J. Schneider, M. D. Willis, T. Klimach, F. Helleis, H. Bozem, D. Kunkel, P. Hoor, J. Burkart, W. R. Leaitch, A. A. Aliabadi, J. P. D. Abbatt, A. B. Herber and S. Borrmann, Particulate trimethylamine in the summertime Canadian high Arctic lower troposphere, *Atmos. Chem. Phys.*, 2017, **17**, 13747-13766.
140. M. D. Willis, J. Burkart, J. L. Thomas, F. Kollner, J. Schneider, H. Bozem, P. M. Hoor, A. A. Aliabadi, H. Schulz, A. B. Herber, W. R. Leaitch and J. P. D. Abbatt, Growth of nucleation mode particles in the summertime Arctic: a case study, *Atmos. Chem. Phys.*, 2016, **16**, 7663-7679.

141. C. Muller, Y. Iinuma, J. Karstensen, D. van Pinxteren, S. Lehmann, T. Gnauk and H. Herrmann, Seasonal variation of aliphatic amines in marine sub-micrometer particles at the Cape Verde islands, *Atmos. Chem. Phys.*, 2009, **9**, 9587-9597.
142. L. Ampollini, E. F. Katz, S. Bourne, Y. Tian, A. Novoselac, A. H. Goldstein, G. Lucic, M. S. Waring and P. F. DeCarlo, Observations and contributions of real-time indoor ammonia concentrations during HOMEChem, *Environ. Sci. Technol.*, 20019, **53**, 8591-8598.
143. F. M. Schmidt, O. Vaittinen, M. Metsala, M. Lehto, C. Forsblom, P. Groop and L. Halonen, Ammonia in breath and emitted from skin, *J. Breath Res.*, 2013, **7**, 1-14.
144. M. A. Sutton, U. Dragosits, Y. S. Tang and D. Fowler, Ammonia emissions from non-agricultural sources in the UK, *Atmos. Environ.*, 2000, **34**, 855-869.
145. H. H. Chen, M. J. Ezell, K. D. Arquero, M. E. Varner, M. L. Dawson, R. B. Gerber and B. J. Finlayson-Pitts, Correction: New particle formation and growth from methanesulfonic acid, trimethylamine and water, *Phys. Chem. Chem. Phys.*, 2017, **19**, 4893-4893.
146. K. Neitola, D. Brus, U. Makkonen, M. Sipila, H. Lihavainen and M. Kulmala, Effect of addition of four base compounds on sulphuric-acid-water new-particle formation: a laboratory study, *Boreal Environ. Res.*, 2014, **19**, 257-274.
147. M. J. Ezell, H. Chen, K. D. Arquero and B. J. Finlayson-Pitts, Aerosol fast flow reactor for laboratory studies of new particle formation, *J. Aerosol Sci.*, 2014, **78**, 30-40.
148. J. Vanhanen, J. Mikkila, K. Lehtipalo, M. Sipila, H. E. Manninen, E. Siivola, T. Petaja and M. Kulmala, Particle size magnifier for nano-CN detection, *Aerosol Sci. Technol.*, 2011, **45**, 533-542.
149. J. Kangasluoma, H. Junninen, K. Lehtipalo, J. Mikkila, J. Vanhanen, M. Attoui, M. Sipila, D. Worsnop, M. Kulmala and T. Petaja, Remarks on ion generation for CPC detection efficiency studies in sub-3-nm size range, *Aerosol Sci. Technol.*, 2013, **47**, 556-563.
150. J. Kangasluoma, C. Kuang, D. Wimmer, M. P. Rissanen, K. Lehtipalo, M. Ehn, D. R. Worsnop, J. Wang, M. Kulmala and T. Petaja, Sub-3 nm particle size and composition dependent response of a nano-CPC battery, *Atmos. Meas. Tech.*, 2014, **7**, 689-700.
151. D. Wimmer, K. Lehtipalo, A. Franchin, J. Kangasluoma, F. Kreissl, A. Kurten, A. Kupc, A. Metzger, J. Mikkila, T. Petaja, F. Riccobono, J. Vanhanen, M. Kulmala and J. Curtius, Performance of diethylene glycol-based particle counters in the sub-3 nm size range, *Atmos. Meas. Tech.*, 2013, **6**, 1793-1804.
152. M. Hermann, B. Wehner, O. Bischof, H. S. Han, T. Krinke, W. Liu, A. Zerrath and A. Wiedensohler, Particle counting efficiencies of new TSI condensation particle counters, *J. Aerosol Sci.*, 2007, **38**, 674-682.
153. A. Kupc, O. Bischof, T. Tritscher, M. Beeston, T. Krinke and P. E. Wagner, Laboratory characterization of a new nano-water-based CPC 3788 and performance comparison to an ultrafine butanol-based CPC 3776, *Aerosol Sci. Technol.*, 2013, **47**, 183-191.
154. J. Xu, V. Perraud, B. J. Finlayson-Pitts and R. B. Gerber, Uptake of water by an acid-base nanoparticle: theoretical and experimental studies of the methanesulfonic acid-methylamine system, *Physical Chemistry Chemical Physics*, 2018, **20**, 22249-22259.
155. M. L. Dawson, M. E. Varner, V. Perraud, M. J. Ezell, J. Wilson, A. Zelenyuk, R. B. Gerber and B. J. Finlayson-Pitts, Amine-amine exchange in aminium-methanesulfonate aerosols, *Journal of Physical Chemistry C*, 2014, **118**, 29431-29440.

156. J. Xu, B. J. Finlayson-Pitts and R. B. Gerber, Nanoparticles grown from methanesulfonic acid and methylamine: microscopic structures and formation mechanism, *Phys. Chem. Chem. Phys.*, 2017, **19**, 31949-31957.
157. E. Burrell, T. Kar and J. C. Hansen, Computational study of the thermodynamics of new particle foramtion initiated by complexes of $H_2SO_4$-$H_2O$-$NH_x$, $CH_3SO_3H$-$H_2O$-$NH_x$, and $HO_2$-$H_2O$-$NH_x$, *ACS Earth Space Chem.*, 2019, **3**, 1415-1425.
158. N. Myllys, T. Olenius, T. Kurten, H. Vehkamaki, I. Riipinen and J. Elm, Effect of bisulfate, ammonia, and ammonium on the clustering of organic acids and sulfuric acid, *J. Phys. Chem. A*, 2017, **121**, 4812-4824.
159. A. B. Nadykto, F. Q. Yu, M. V. Jakovleva, J. Herb and Y. S. Xu, Amines in the Earth's atmosphere: a density functional theory study of the thermochemistry of pre-nucleation clusters, *Entropy*, 2011, **13**, 554-569.
160. S. S. Lv, S. K. Miao, Y. Ma, M. M. Zhang, Y. Wen, C. Y. Wang, Y. P. Zhu and W. Huang, Properties and atmospheric implication of methylamine sulfuric acid-water clusters, *J. Phys. Chem. A*, 2015, **119**, 8657-8666.
161. A. D. Becke, Density-functional thermochemistry .3. The role of exact exchange, *J. Chem. Phys.*, 1993, **98**, 5648-5652.
162. R. G. Parr, *Density-Functional Theory of Atoms and Molecules*, Oxford University Press, 1994.
163. J. P. Perdew, J. A. Chevary, S. H. Vosko, K. A. Jackson, M. R. Pederson, D. J. Singh and C. Fiolhais, Atoms, Molecules, Solids, and Surfaces - Applications of the Generalized Gradient Approximation for Exchange and Correlation, *Phys. Rev. B*, 1992, **46**, 6671-6687.
164. S. Grimme, J. Antony, S. Ehrlich and H. Krieg, A consistent and accurate ab initio parametrization of density functional dispersion correction (DFT-D) for the 94 elements H-Pu, *J. Chem. Phys.*, 2010, **132**, Artn 154104, doi: 154110.151063/154101.3382344.
165. T. Kurten, M. Noppel, H. Vehkamaki, M. Salonen and M. Kulmala, Quantum chemical studies of hydrate formation of H2SO4 and HSO4-, *Boreal Environ. Res.*, 2007, **12**, 431-453.
166. J. P. Devlin, J. Sadlej, M. Hollman and V. Buch, Solvation stages of HCl and HBr in crystalline phases with methanol and small ethers: Acid-ether cluster complexes in amorphous and crystal phases, *J. Phys. Chem. A*, 2004, **108**, 2030-2043.
167. S. S. Xantheas, Ab-initio studies of cyclic water clusters $(H_2O)_n$, n=1-6 - III. Comparison of density-functional with MP2 results, *J. Chem. Phys.*, 1995, **102**, 4505-4517.
168. Y. Miller, G. M. Chaban, J. Zhou, K. R. Asmis, D. M. Neumark and R. B. Gerber, Vibrational spectroscopy of $(SO_4^{2-})\cdot(H_2O)_n$ clusters, n=1-5: Harmonic and anharmonic calculations and experiment, *J. Chem. Phys.*, 2007, **127**, Artn 094305, doi: 094310.091063/094301.2764074.
169. G. R. Medders, V. Babin and F. Paesani, A critical assessment of two-body and three-body interactions in water, *J. Chem. Theory Comput.*, 2013, **9**, 1103-1114.
170. J. M. Martinez and L. Martinez, Packing optimization for automated generation of complex system's initial configurations for molecular dynamics and docking, *J. Comput. Chem.*, 2003, **24**, 819-825.
171. L. Martinez, R. Andrade, E. G. Birgin and J. M. Martinez, PACKMOL: A package for building initial configurations for molecular dynamics simulations, *J. Comput. Chem.*, 2009, **30**, 2157-2164.

172. J. P. Foster and F. Weinhold, Natural hybrid orbitals, *J. Amer. Chem. Soc.*, 1980, **102**, 7211-7218.
173. A. E. Reed and F. Weinhold, Natural bond orbital analysis of near-Hartree-Fock water dimer, *J. Chem. Phys.*, 1983, **78**, 4066-4073.
174. Y. H. Shao, Z. T. Gan, E. Epifanovsky, A. T. B. Gilbert, M. Wormit, J. Kussmann, A. W. Lange, A. Behn, J. Deng, X. T. Feng, D. Ghosh, M. Goldey, P. R. Horn, L. D. Jacobson, I. Kaliman, R. Z. Khaliullin, T. Kus, A. Landau, J. Liu, E. I. Proynov, Y. M. Rhee, R. M. Richard, M. A. Rohrdanz, R. P. Steele, E. J. Sundstrom, H. L. Woodcock, P. M. Zimmerman, D. Zuev, B. Albrecht, E. Alguire, B. Austin, G. J. O. Beran, Y. A. Bernard, E. Berquist, K. Brandhorst, K. B. Bravaya, S. T. Brown, D. Casanova, C. M. Chang, Y. Q. Chen, S. H. Chien, K. D. Closser, D. L. Crittenden, M. Diedenhofen, R. A. DiStasio, H. Do, A. D. Dutoi, R. G. Edgar, S. Fatehi, L. Fusti-Molnar, A. Ghysels, A. Golubeva-Zadorozhnaya, J. Gomes, M. W. D. Hanson-Heine, P. H. P. Harbach, A. W. Hauser, E. G. Hohenstein, Z. C. Holden, T. C. Jagau, H. J. Ji, B. Kaduk, K. Khistyaev, J. Kim, J. Kim, R. A. King, P. Klunzinger, D. Kosenkov, T. Kowalczyk, C. M. Krauter, K. U. Lao, A. D. Laurent, K. V. Lawler, S. V. Levchenko, C. Y. Lin, F. Liu, E. Livshits, R. C. Lochan, A. Luenser, P. Manohar, S. F. Manzer, S. P. Mao, N. Mardirossian, A. V. Marenich, S. A. Maurer, N. J. Mayhall, E. Neuscamman, C. M. Oana, R. Olivares-Amaya, D. P. O'Neill, J. A. Parkhill, T. M. Perrine, R. Peverati, A. Prociuk, D. R. Rehn, E. Rosta, N. J. Russ, S. M. Sharada, S. Sharma, D. W. Small, A. Sodt, T. Stein, D. Stuck, Y. C. Su, A. J. W. Thom, T. Tsuchimochi, V. Vanovschi, L. Vogt, O. Vydrov, T. Wang, M. A. Watson, J. Wenzel, A. White, C. F. Williams, J. Yang, S. Yeganeh, S. R. Yost, Z. Q. You, I. Y. Zhang, X. Zhang, Y. Zhao, B. R. Brooks, G. K. L. Chan, D. M. Chipman, C. J. Cramer, W. A. Goddard, M. S. Gordon, W. J. Hehre, A. Klamt, H. F. Schaefer, M. W. Schmidt, C. D. Sherrill, D. G. Truhlar, A. Warshel, X. Xu, A. Aspuru-Guzik, R. Baer, A. T. Bell, N. A. Besley, J. D. Chai, A. Dreuw, B. D. Dunietz, T. R. Furlani, S. R. Gwaltney, C. P. Hsu, Y. S. Jung, J. Kong, D. S. Lambrecht, W. Z. Liang, C. Ochsenfeld, V. A. Rassolov, L. V. Slipchenko, J. E. Subotnik, T. Van Voorhis, J. M. Herbert, A. I. Krylov, P. M. W. Gill and M. Head-Gordon, Advances in molecular quantum chemistry contained in the Q-Chem 4 program package, *Mol. Phys.*, 2015, **113**, 184-215.
175. E. P. L. Hunter and S. G. Lias, Evaluated gas phase basicities and proton affinities of molecules: An update, *J. Phys. Chem. Ref. Data*, 1998, **27**, 413-656.
176. W. R. Leaitch, S. Sharma, L. Huang, D. Toom-Sauntry, A. Chivulescu, A.-M. Macdonald, K. von Salzen, J. R. Pierce, A. K. Bertram, J. C. Schroder, N. C. Shantz, R. Y.-W. Chang and A.-L. Norman, Dimethyl sulfide control of the clean summertime Arctic aerosol and cloud, *Elementa Sci. Anthrop.*, 2013, **1**, 1-12.
177. P. K. Quinn, T. L. Miller, T. S. Bates, J. A. Ogren, E. Andrews and G. E. Shaw, A 3-year record of simultaneously measured aerosol chemical and optical properties at Barrow, Alaska, *J. Geophys. Res.*, 2002, **107**, Artn 4130, doi: 4110.1029/2001jd001248.
178. J. Burkart, M. D. Willis, H. Bozem, J. L. Thomas, K. Law, P. Hoor, A. A. Aliabadi, F. Kollner, J. Schneiders, A. Herber, J. P. D. Abbatt and W. R. Leaitch, Summertime observations of elevated levels of ultrafine particles in the high Arctic marine boundary layer, *Atmos. Chem. Phys.*, 2017, **17**, 5515-5535.
179. S. Sharma, E. Chan, M. Ishizawa, D. Toom-Sauntry, S. L. Gong, S. M. Li, D. W. Tarasick, W. R. Leaitch, A. Norman, P. K. Quinn, T. S. Bates, M. Levasseur, L. A. Barrie and W. Maenhaut, Influence of transport and ocean ice extent on biogenic aerosol sulfur

in the Arctic atmosphere, *J. Geophys. Res.*, 2012, **117**, Artn D12209, doi: 12210.11029/12011jd017074.

180. S. Trabue, K. Scoggin, L. McConnell, R. Maghirang, E. Razote and J. Hatfield, Identifying and tracking key odorants from cattle feedlots, *Atmos. Environ.*, 2011, **45**, 4243-4251.

181. A. Feilberg, D. Z. Liu, A. P. S. Adamsen, M. J. Hansen and K. E. N. Jonassen, Odorant Emissions from Intensive Pig Production Measured by Online Proton-Transfer-Reaction Mass Spectrometry, *Environ. Sci. Technol.*, 2010, **44**, 5894-5900.

182. J. Filipy, B. Rumburg, G. Mount, H. Westberg and B. Lamb, Identification and quantification of volatile organic compounds from a dairy, *Atmos. Environ.*, 2006, **40**, 1480-1494.

183. A. Sorooshian, E. Crosbie, L. C. Maudlin, J. S. Youn, Z. Wang, T. Shingler, A. M. Ortega, S. Hersey and R. K. Woods, Surface and airborne measurements of organosulfur and methanesulfonate over the western United States and coastal areas, *J. Geophys. Res.*, 2015, **120**, 8535-8548.

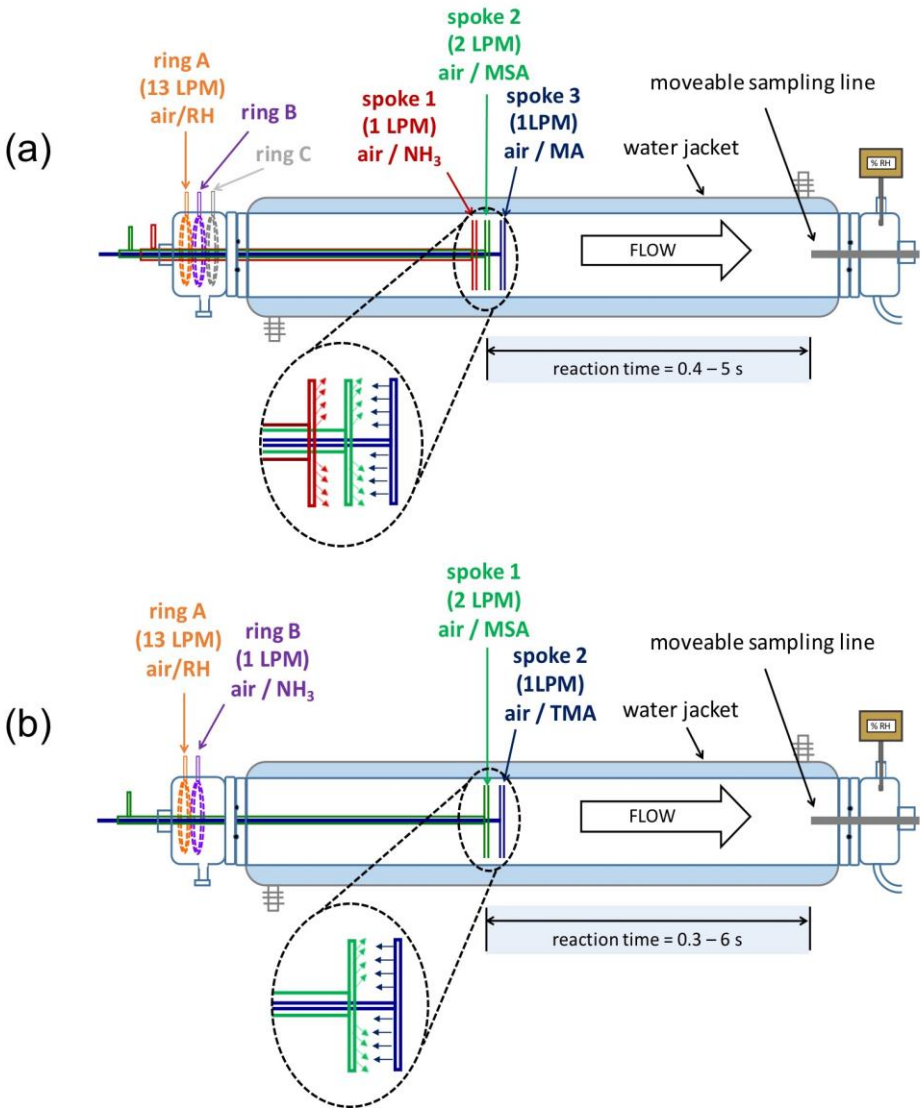


**Figure 1.** Schematics of the flow reactors used to investigate new particle formation from (a) the MSA+MA (±$NH_3$) reaction and (b) the MSA+TMA (±$NH_3$) reaction. The diagrams are adapted from ref. 73 and 147.

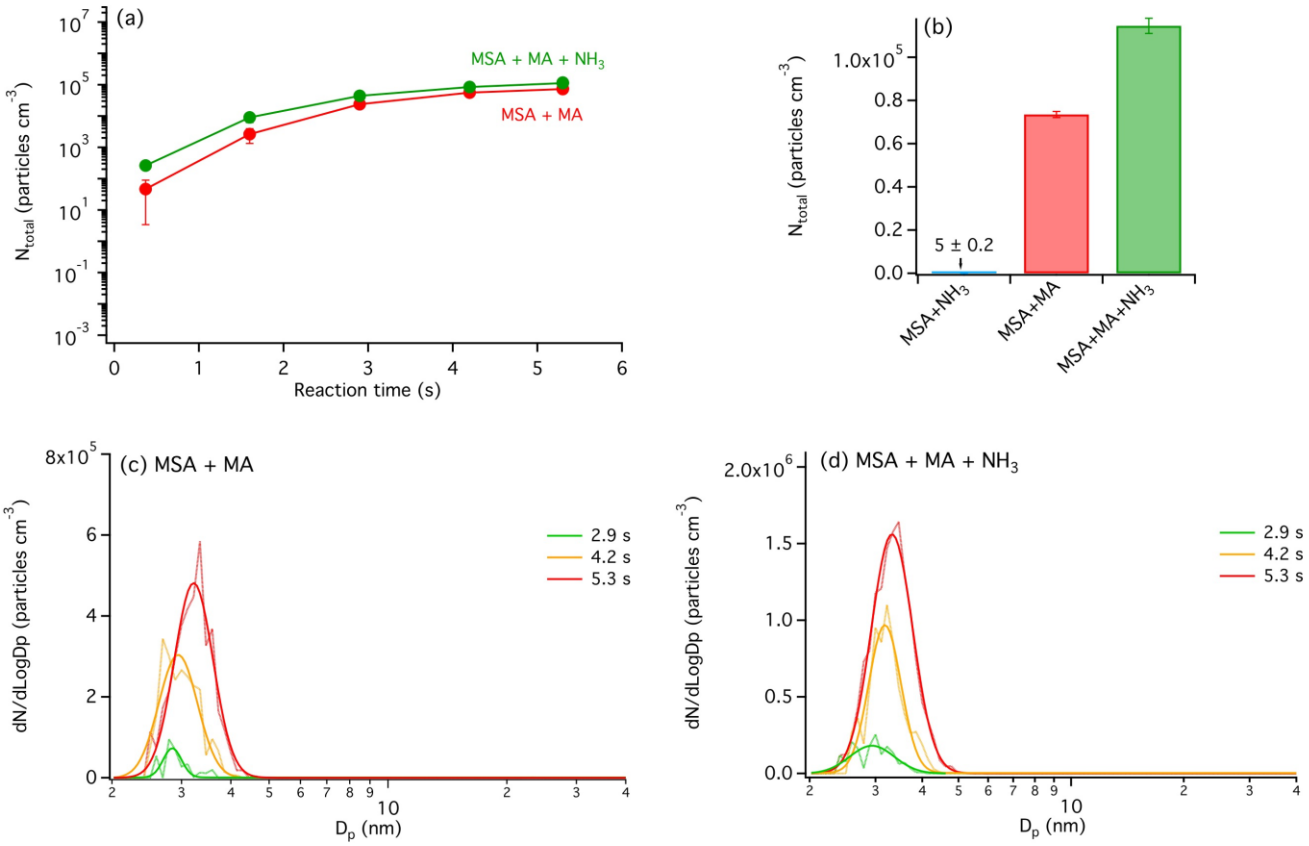


**Figure 2.** (a) Total particle number concentrations ($N_{total}$) from MSA+MA and MSA+MA+$NH_3$ reactions as a function of reaction time measured using the CPC (dry conditions). Each data point corresponds to the average $N_{total}$ measured over a 5-min scan (error bars correspond to 1 standard deviation). (b) Comparison of $N_{total}$ values measured at 5.3 s for MSA+$NH_3$, MSA+MA and MSA+MA+$NH_3$. Size distributions measured using the SMPS are presented in (c) for the MSA+MA and (d) for the MSA+MA+$NH_3$ reactions respectively. Each size distribution is given in light colors with a log normal fit to guide the eye (each distribution corresponds to an average from five successive scans, except for reaction time 5.3 s where ten scans were averaged instead (standard deviation are not shown for clarity)). Concentrations of reactants for all panels are [MSA] = $6.4 \times 10^{10}$ molecules $cm^{-3}$; [MA] = 0 or $6.1 \times 10^{10}$ molecules $cm^{-3}$; [$NH_3$] = 0 or $2.9 \times 10^{11}$ molecules $cm^{-3}$.

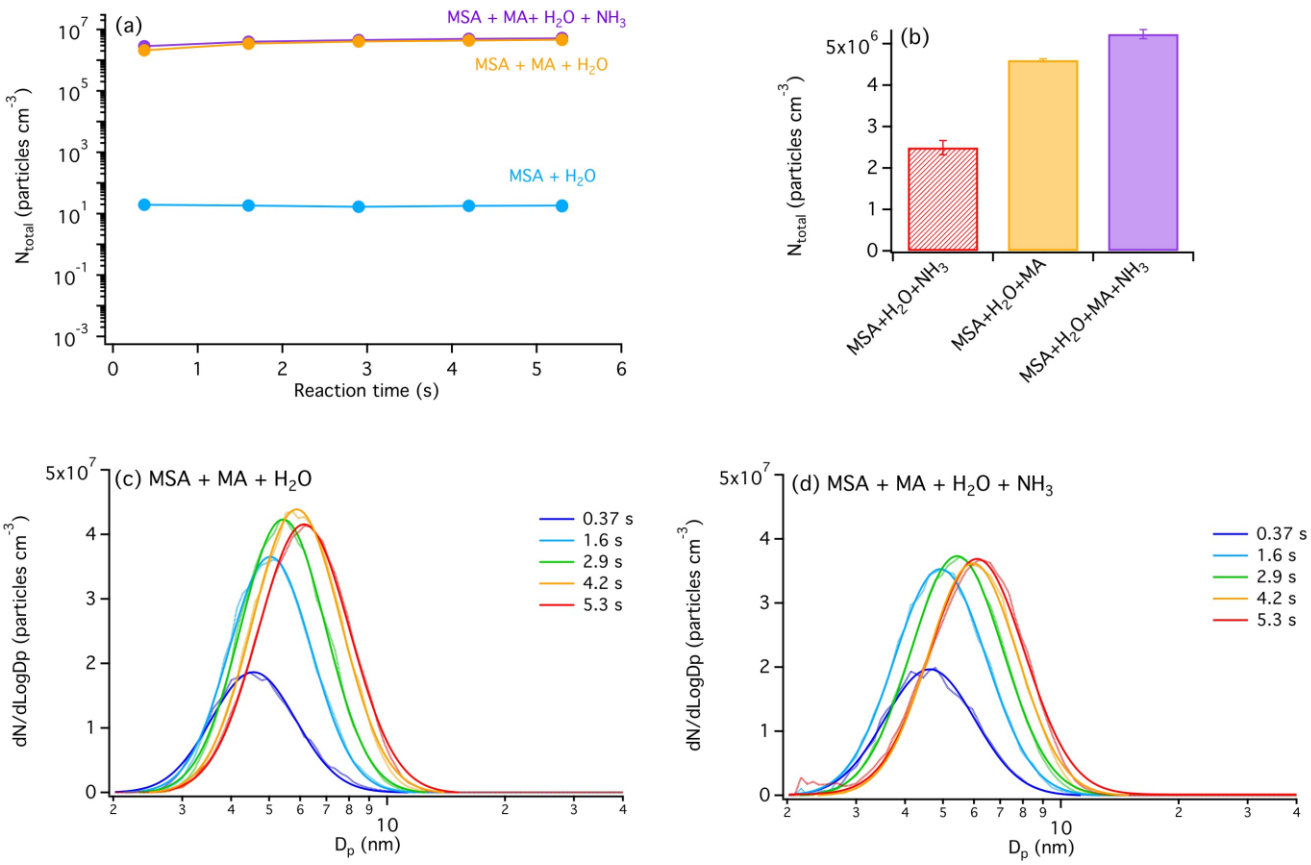


**Figure 3.** (a) Total particle number concentrations ($N_{total}$) from MSA+$H_2O$, MSA+MA+$H_2O$ and MSA+MA+$H_2O$+$NH_3$ reactions as a function of reaction time measured using the CPC (RH ~45-50%). Each data point corresponds to the average $N_{total}$ measured over a 5-min scan (error bars correspond to 1 standard deviation). (b) Comparison of $N_{total}$ values measured at 5.3 s for MSA+$H_2O$+$NH_3$, MSA+$H_2O$+MA and MSA+$H_2O$+MA+$NH_3$. Size distributions measured using the SMPS are presented in (c) for the MSA+MA+$H_2O$ and (d) for the MSA+MA+$H_2O$+$NH_3$ reactions respectively. Each size distribution is given in light colors with a log normal fit to guide the eye (each distribution corresponds to an average from five successive scans, except for reaction time 5.3 s where ten scans were averaged instead (the standard deviation is not shown for clarity)). Concentrations of reactants for all panels are [MSA] = $6.4 \times 10^{10}$ molecules $cm^{-3}$; [MA] = 0 or $6.1 \times 10^{10}$ molecules $cm^{-3}$; [$NH_3$] = 0 or $2.9 \times 10^{11}$ molecules $cm^{-3}$.

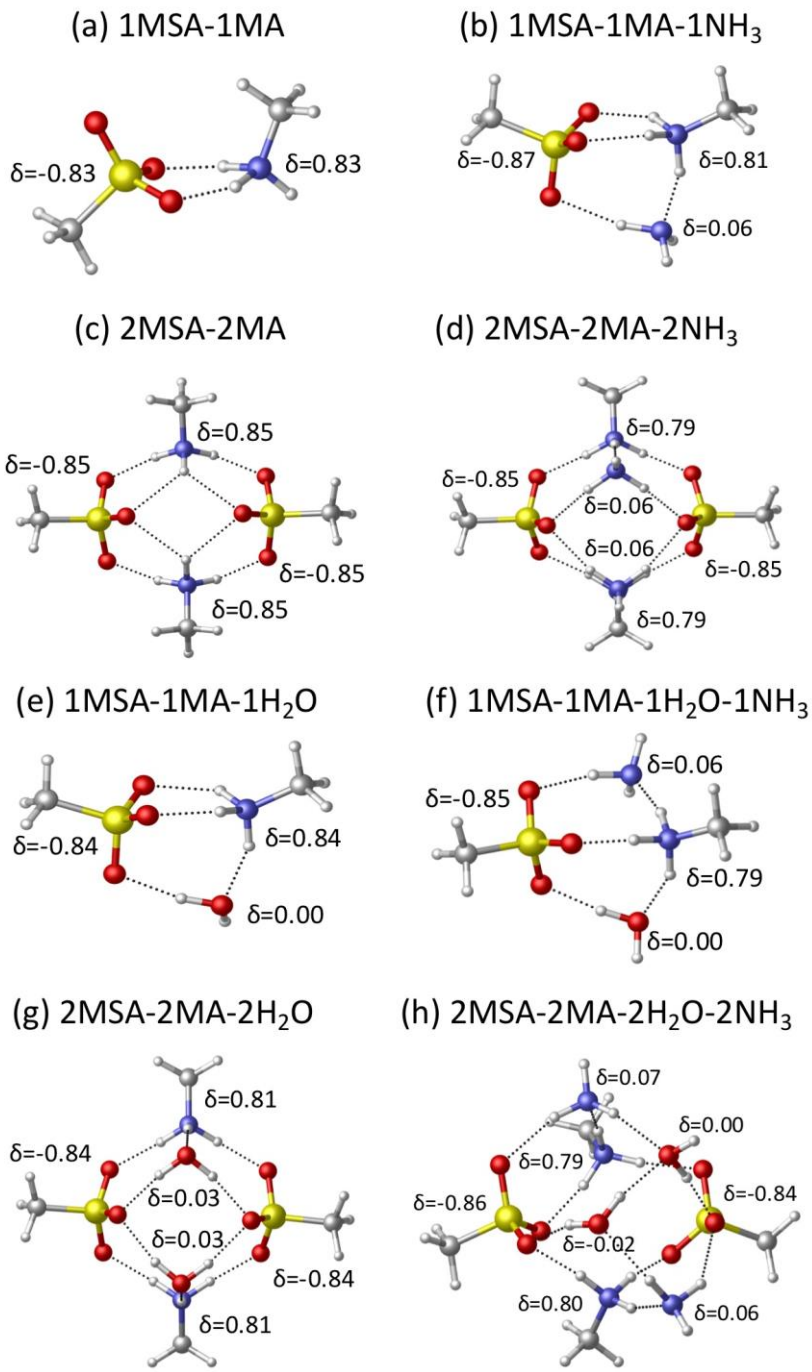


**Figure 4.** Structures with distances (in angstroms) and partial charges δ (in atomic units) of the most stable structures of complexes composed of MSA, MA, $NH_3$ and $H_2O$ at the level of B3LYP-D3/aug-cc-pVDZ.

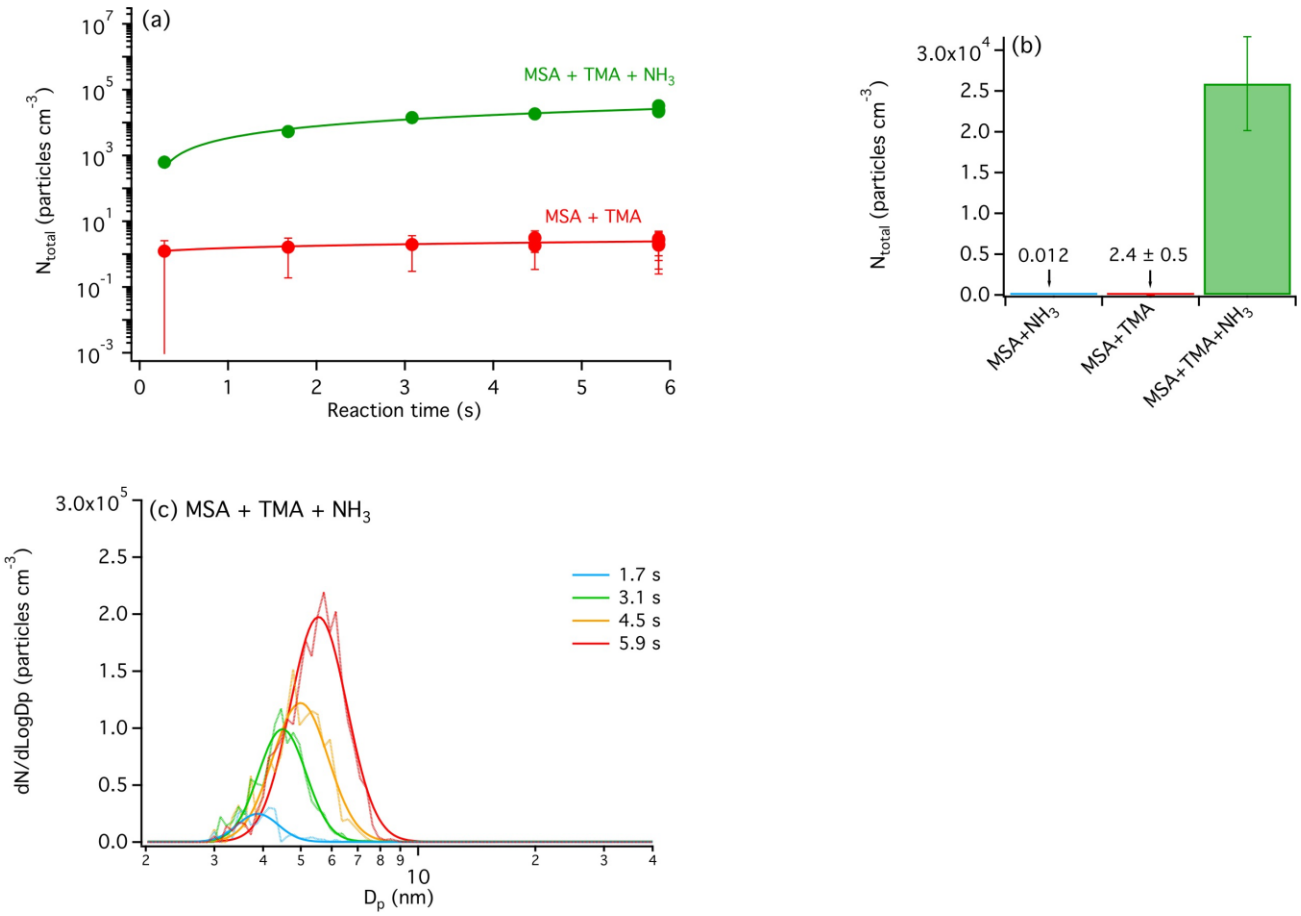


**Figure 5.** (a) Total particle number concentrations ($N_{total}$) from MSA+TMA and MSA+TMA+$NH_3$ reaction systems as a function of reaction time measured using the CPC (dry conditions). Each data point corresponds to the average $N_{total}$ measured over a 5-min scan (error bars correspond to 1 standard deviation). (b) Comparison of $N_{total}$ values measured at 5.9 s for MSA+$NH_3$, MSA+TMA and MSA+TMA+$NH_3$. (c) Size distribution for the MSA+TMA+$NH_3$ reaction. (The MSA+TMA reaction didn't generate enough particles to be observable by the SMPS). Each size distribution is given in light colors with a log normal fit to guide the eye (each distribution corresponds to an average from five successive scans, except for reaction time 5.9 s where ten scans were averaged (standard deviation are not shown for clarity)). Concentrations of reactants for all panels are [MSA] = $7.9 \times 10^{10}$ molecules $cm^{-3}$; [TMA] = 0 or $5.0 \times 10^{10}$ molecules $cm^{-3}$; [$NH_3$] = 0 or $2.2 \times 10^{10}$ molecules $cm^{-3}$. Note that at 0.28 s, particles (> 2.0 nm) were not detectable using the SMPS for the MSA+TMA+$NH_3$ reaction.

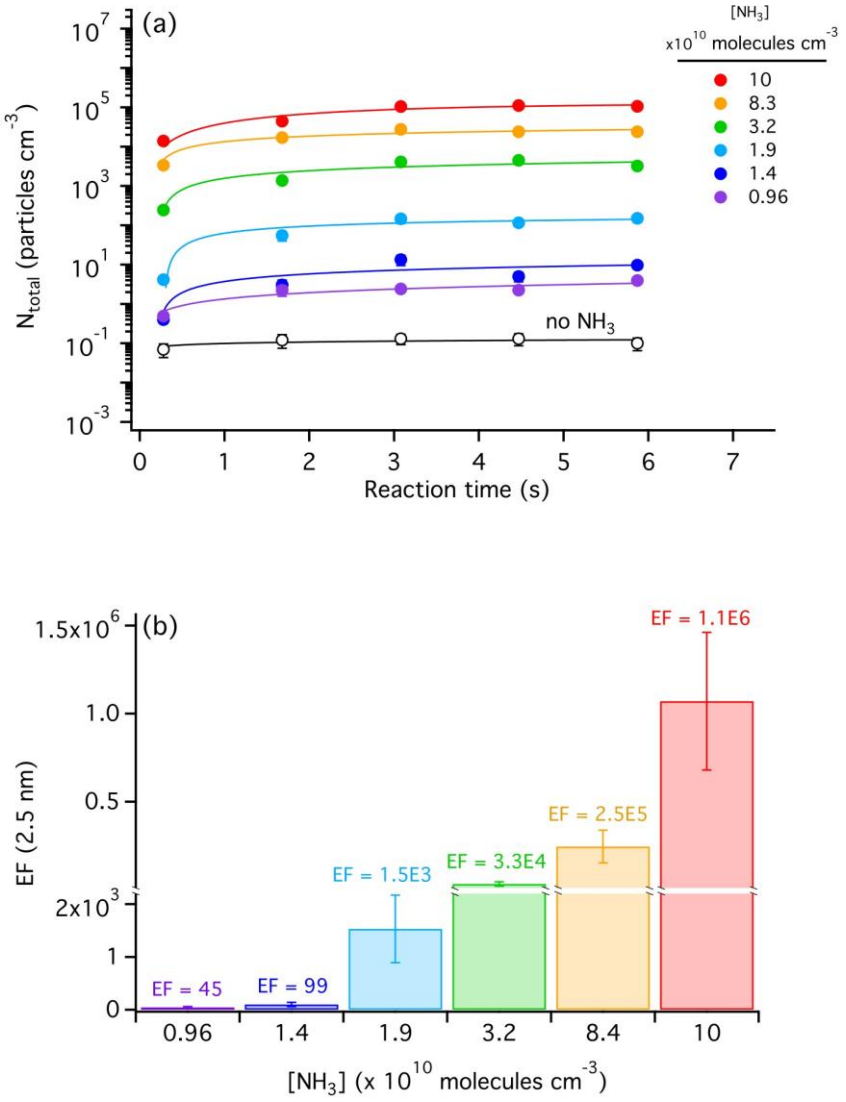


**Figure 6.** (a) Total particle concentrations ($N_{total}$) from MSA+TMA+$NH_3$ reactions for varying $NH_3$ concentrations as a function of reaction time measured using the CPC (dry conditions; each point corresponds to an average from three replicate CPC measurements ± 1 standard deviation). (b) Enhancement factor for particles measured as a function of $NH_3$ concentration (data for t = 5.9 s). Concentrations of reactants are [MSA] = $6.4 \times 10^{10}$ molecules $cm^{-3}$; [TMA] = $4.8 \times 10^{10}$ molecules $cm^{-3}$; [$NH_3$] = $(0\text{-}10) \times 10^{10}$ molecules $cm^{-3}$.

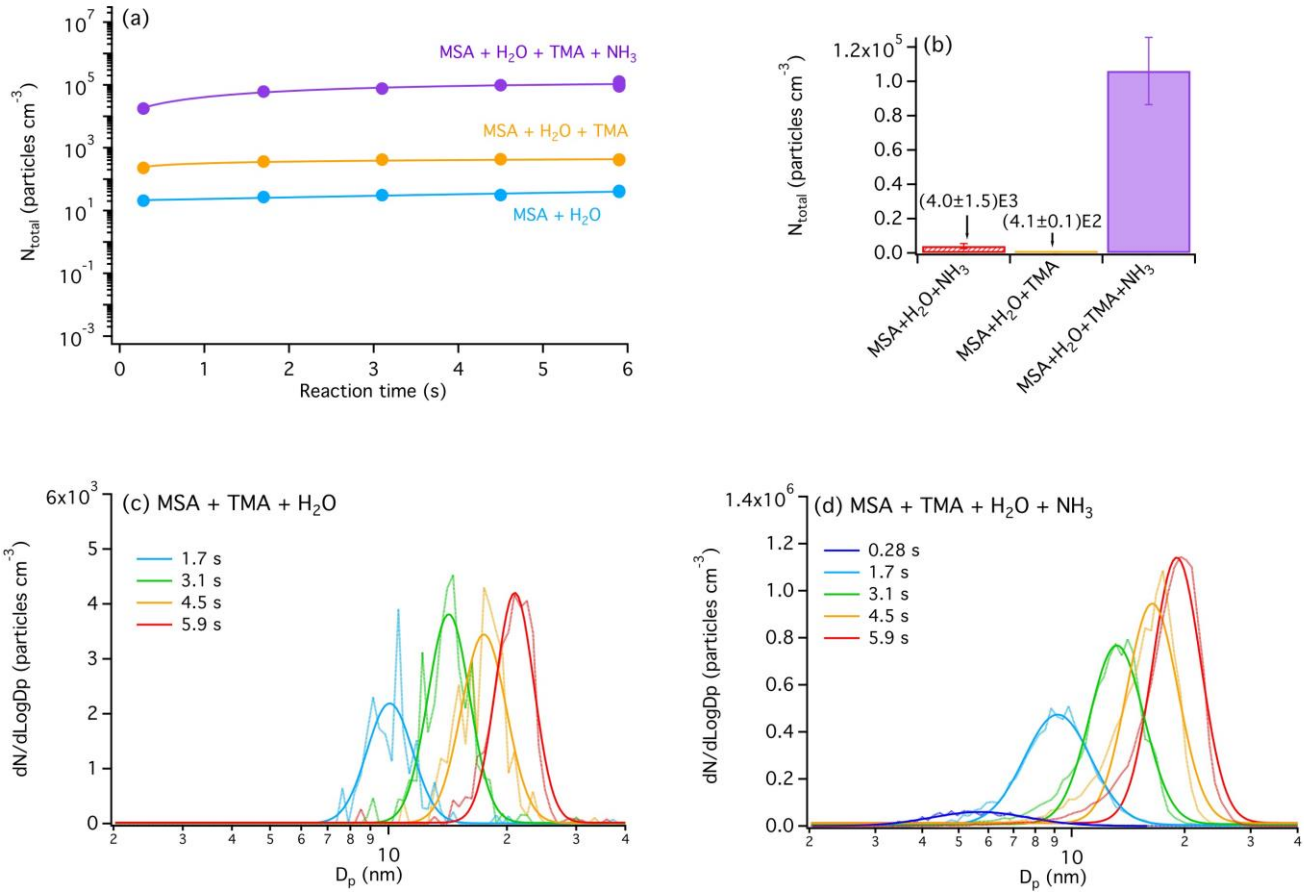


**Figure 7.** (a) Total particle number concentrations ($N_{total}$) from MSA+TMA+$H_2O$ and MSA+TMA+$NH_3$+$H_2O$ reactions as a function of reaction time measured using the CPC (RH ~45-50%). Each data point corresponds to the average $N_{total}$ measured over a 5-min scan (error bars correspond to 1 standard deviation). (b) Comparison of $N_{total}$ values measured at 5.9 s for MSA+$H_2O$+$NH_3$, MSA+$H_2O$+TMA and MSA+$H_2O$+TMA+$NH_3$. Corresponding size distributions for (c) the MSA+TMA+$H_2O$ reaction and (d) the MSA+TMA+$H_2O$+$NH_3$ reactions, respectively. Each size distribution is given in light colors with a log normal fit to guide the eye (each distribution corresponds to an average from five successive scans, except for reaction time 5.9 s where ten scans were averaged instead (standard deviation are not shown for clarity)). Concentrations of reactants for all panels are [MSA] = $7.9 \times 10^{10}$ molecules $cm^{-3}$; [TMA] = 0 or $5.0 \times 10^{10}$ molecules $cm^{-3}$; [$NH_3$] = 0 or $2.2 \times 10^{10}$ molecules $cm^{-3}$.

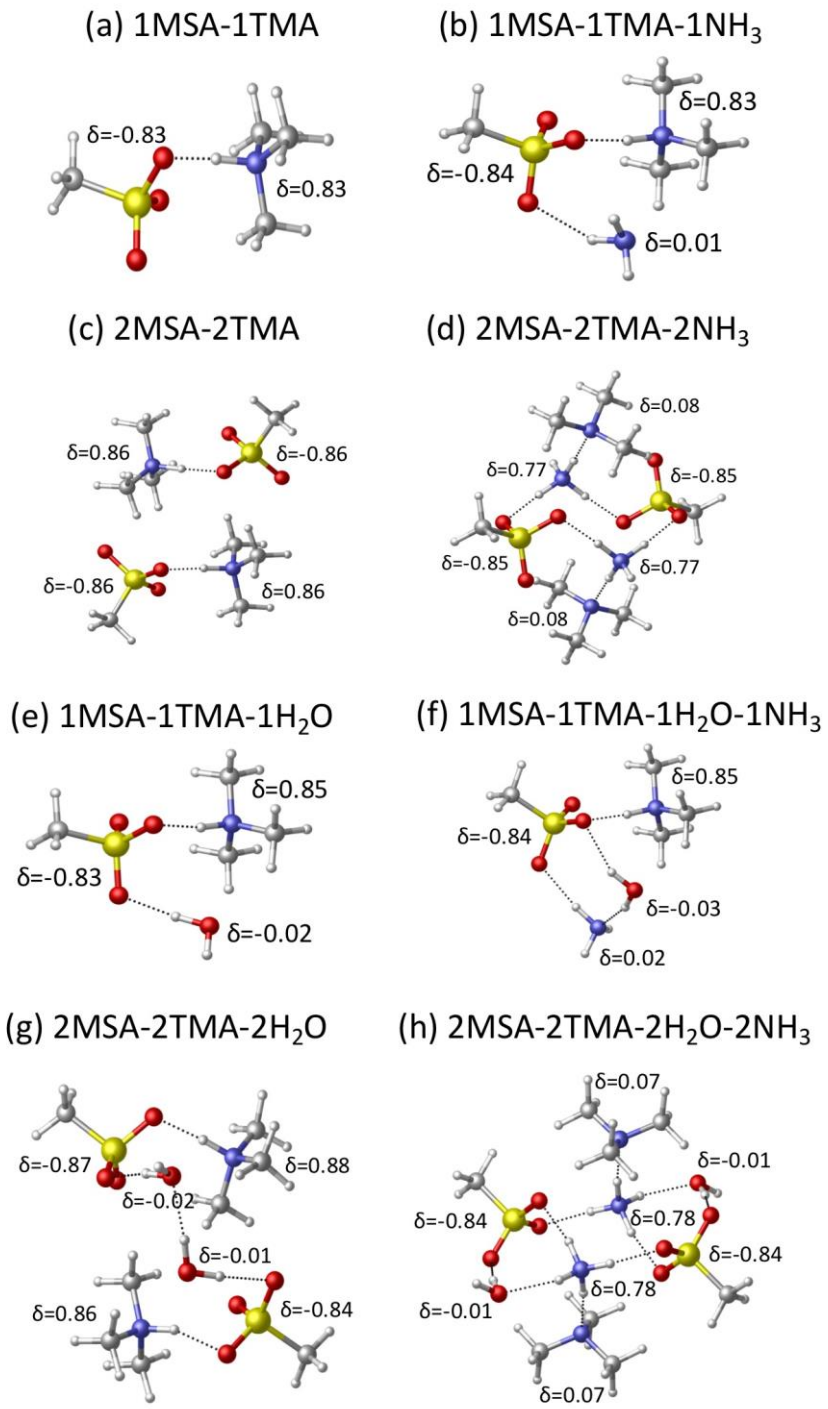


**Figure 8.** Structures with distances (in angstroms) and partial charges δ (in atomic units) of the most stable structures of complexes composed of MSA, TMA, $NH_3$ and $H_2O$ at the level of B3LYP-D3/aug-cc-pVDZ.

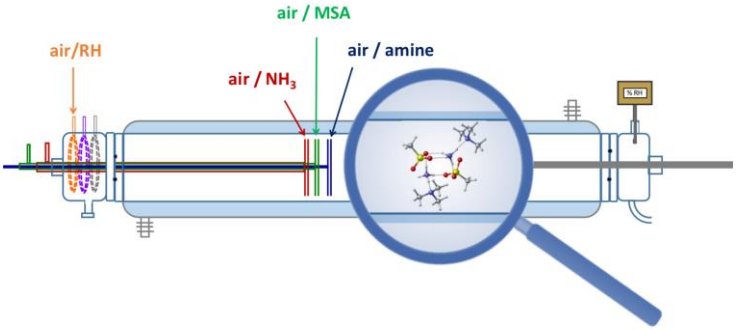


Particle formation from methanesulfonic acid-amine multicomponent systems is investigated using a combined experimental and theoretical approach.